

Colorful Pinball: Density-Weighted Quantile Regression for Conditional Guarantee of Conformal Prediction

Qianyi Chen¹, Bo Li^{1*}

¹School of Economics and Management, Tsinghua University

cqy22@mails.tsinghua.edu.cn

libo@sem.tsinghua.edu.cn

Abstract

While conformal prediction provides robust marginal coverage guarantees, achieving reliable conditional coverage for specific inputs remains challenging. Although exact distribution-free conditional coverage is impossible with finite samples, recent work has focused on improving the conditional coverage of standard conformal procedures. Distinct from approaches that target relaxed notions of conditional coverage, we directly minimize the mean squared error of conditional coverage by refining the quantile regression components that underpin many conformal methods. Leveraging a Taylor expansion, we derive a sharp surrogate objective for quantile regression: a density-weighted pinball loss, where the weights are given by the conditional density of the conformity score evaluated at the true quantile. We propose a three-headed quantile network that estimates these weights via finite differences using auxiliary quantile levels at $1 - \alpha \pm \delta$, subsequently fine-tuning the central quantile by optimizing the weighted loss. We provide a theoretical analysis with exact non-asymptotic guarantees characterizing the resulting excess risk. Extensive experiments on diverse high-dimensional real-world datasets demonstrate remarkable improvements in conditional coverage performance.

1 Introduction

As machine learning systems are increasingly deployed in high-stakes environments, the demand for reliability extends beyond predictive accuracy to rigorous uncertainty quantification (UQ). In safety-critical domains, a model’s ability to provide appropriate predictive intervals is often as valuable as accurate point predictions. Among existing UQ frameworks, Conformal Prediction (CP; [Vovk et al., 2005](#), [Shafer and Vovk, 2008](#)) has emerged as a paradigm of choice due to its mathematically grounded guarantees. Unlike Bayesian methods or ensemble techniques that often rely on strong distributional assumptions or heavy computational overhead, CP offers a distribution-free, model-agnostic framework. It constructs prediction sets or intervals that provably contain the ground truth with a user-specified probability $1 - \alpha$ (e.g., 90%) in finite samples, providing a layer of statistical trust that is indispensable for real-world deployment.

However, standard split conformal prediction only provides a marginal guarantee over the population and cannot guarantee conditional coverage for specific instances—precisely what practitioners require in high-stakes scenarios. Although hardness results for exact distribution-free conditional guarantees with finite

*Corresponding author

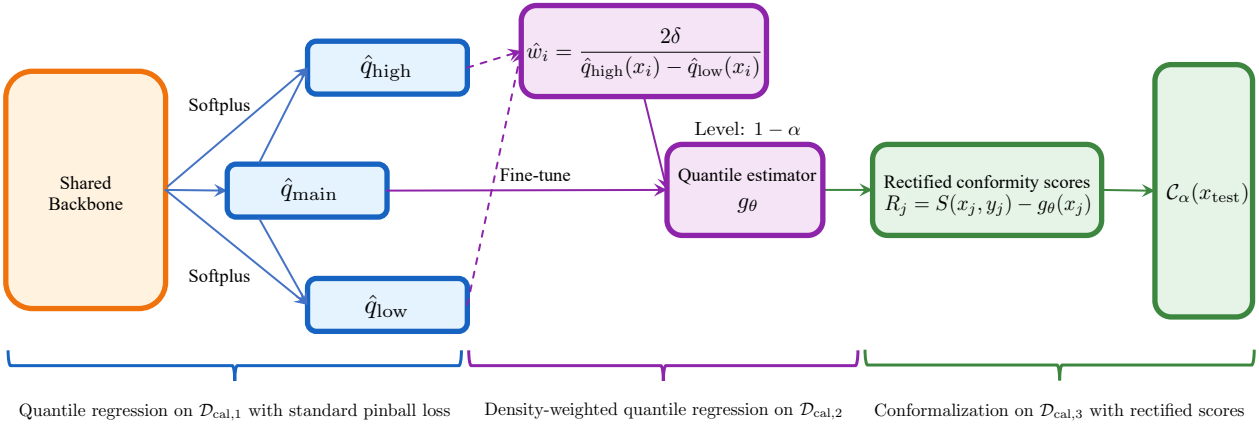


Figure 1: **Illustration of the Colorful Pinball Conformal Prediction framework.** We estimate density-based weights via auxiliary quantiles, fine-tune the central quantile with density-weighted pinball loss, and apply conformalization with rectified conformity scores.

samples are well-established [Vovk \[2012\]](#), [Lei and Wasserman \[2014\]](#), [Foygel Barber et al. \[2021\]](#), a growing body of works targets improving the conditional coverage of conformal procedures. To this end, many works explore to relax the conditional requirement [Angelopoulos et al. \[2024\]](#), e.g., group-conditional coverage [Jung et al. \[2023\]](#), [Ding et al. \[2023\]](#).

Instead, this paper targets controlling the exact conditional coverage rather than relaxed forms. A natural objective is the MSE of conditional coverage—termed Mean Squared Conditional Error (MSCE) in [Kiyani et al. \[2024\]](#). We consider this metric since minimizing the MSCE provides high-probability control over conditional coverage deviations via Bernstein’s inequality. We build upon the connection between MSCE and the excess risk of the pinball loss established in recent literature [Kiyani et al. \[2024\]](#), [Plassier et al. \[2025a\]](#). Specifically, these works show that the MSCE is upper-bounded by the excess risk of a quantile estimator with pinball loss, suggesting that improving the quantile estimator directly translates to better conditional coverage.

However, we identify that this standard upper bound is often loose, as it relies on a uniform Lipschitz constant for the conditional cumulative distribution function (CDF) of the nonconformity scores, $F_{S|X}(s)$. Using a Taylor expansion, we derive a significantly sharper approximation of MSCE: the excess risk of the pinball loss weighted by the conditional density of the score evaluated at the true quantile, $f_{S|X}(q(x))$. This formulation reveals the latent heteroscedastic structure within the objective; for instance, in the location-scale family, this weighting term is proportional to the inverse scale, $1/\sigma(x)$.

Motivated by this insight, we propose a three-stage framework named **Colorful Pinball Conformal Prediction (CPCP)**, as shown in Figure 1. Our method first estimates the density-based weights via joint quantile regression, then fine-tunes the target quantile by minimizing the weighted pinball loss, and finally rectifies the original nonconformity scores using the fine-tuned quantile estimator. Theoretically, we establish exact **non-asymptotic** results for the generalization error of weighted risk, which is of broader interest in problems involving estimated reciprocal weights. To ensure robustness, our algorithm incorporates specific mechanisms to mitigate practical issues such as quantile crossing, unstable inverse weights, and Taylor approximation errors, enabling superior performance on extensive benchmarks. In brief, our main contributions are fourfold:

- We identify the inadequacy of naive quantile regression regarding conditional coverage and construct a significantly sharper approximation of the MSCE.

- We propose a principled algorithmic framework to directly minimize the MSCE with carefully designed mechanisms to guarantee practical robustness.
- We develop a non-asymptotic theory on generalization error with estimated reciprocal weights.
- We validate our approach through comprehensive experiments with extensive ablation studies.

1.1 Related Works

We focus our discussion on the conditional coverage of conformal prediction. In the literature, there exists another branch of work concerning the *training-conditional* guarantee [Park et al. \[2020\]](#), [Bian and Barber \[2023\]](#), [Duchi \[2025\]](#), which studies the coverage probability conditional on the specific calibration set observed. To clarify, we are specifically concerned with the coverage guarantee conditional on the covariate of the test sample, X_{test} .

Formally, exact conditional coverage refers to $\mathbb{P}(Y_{\text{test}} \in \mathcal{C}_\alpha(X_{\text{test}}) \mid X_{\text{test}})$, which is the ideal quantity we seek to control. In contrast, relaxed versions target quantities such as $\mathbb{P}(Y \in \mathcal{C}_\alpha(X_{\text{test}}) \mid H(X_{\text{test}}))$ for certain function H .

Group-conditional coverage serves as a natural approximation to the exact conditional guarantee. Here, we specifically discuss the case where groups are formed by partitioning the covariate space. Classic conformal procedures operate with pre-defined groups [Jung et al. \[2023\]](#), where h is a fixed discrete partition function. Beyond fixed groups, [Kiyani et al. \[2024\]](#) propose co-training the partition function with quantile regression within each group, providing a discrete approximation of conditional coverage. Though straightforward, the precision of this discrete approximation is limited, and the convergence rate of the resulting MSCE scales as slowly as $O(n^{-1/4})$. Adopting a different perspective that reformulates the conditional guarantee as moment equations, [Gibbs et al. \[2025a\]](#) extends the approximation to infinite, overlapping groups. They leverage regularized quantile regression as well as full conformal prediction [Vovk et al. \[2005\]](#). However, [Gibbs et al. \[2025a\]](#) provides control only on a substitute metric—coverage under covariate shift—rather than the exact conditional coverage. Moreover, full conformal procedures incur a significant computational burden, limiting their general applicability.

Beyond group-conditional guarantees, localized conformal prediction [Bian and Barber \[2023\]](#), [Hore and Barber \[2024\]](#) provides another avenue to approximate the conditional guarantee by applying kernel weighting during empirical quantile computation. As analyzed in [Hore and Barber \[2024\]](#), the guarantee provided by such localization corresponds to a random function h that outputs a point sampled from a distribution centered at X_{test} , defined by the kernel. However, this strategy suffers inherently from the curse of dimensionality, particularly in the complex, high-dimensional scenarios that modern conformal prediction targets.

Complementing the focus on grouping and quantile computation, a substantial body of literature strives to refine the nonconformity score function. Improving upon the classic residual score, [Lei et al. \[2018\]](#) propose scaled residuals using a learned conditional standard deviation $\sigma(x)$. [Romano et al. \[2019\]](#) propose Conformalized Quantile Regression (CQR), which directly conformalizes two learned quantiles rather than a mean prediction. They also highlighted the difficulty of learning $\sigma(x)$, particularly for overfitted neural networks. More recently, [Xie et al. \[2024\]](#) propose a boosting procedure to iteratively refine the score function. However, besides high computational costs, this method further requires access to training data, which is often infeasible given the prevalence of pre-trained black-box models. Similarly, CQR necessitates replacing the traditional conditional mean regression objective with quantile regression on the training set, thereby

limiting its general applicability. While the aforementioned scores are tailored for one-dimensional labels, another branch of work investigates density-based scores [Izbicki et al. \[2022\]](#), [Plassier et al. \[2025b\]](#), [Braun et al. \[2025a\]](#), which are readily extensible to multi-dimensional labels and also flexible enough to capture heteroscedasticity. However, estimating the conditional density $f(Y | X)$ is generally a harder task than regression on the conditional mean $\mathbb{E}[Y | X]$. Furthermore, the calibration set used for density estimation is typically much smaller than the training set. This sample size mismatch limits the efficacy of density estimation; therefore, in this paper, we focus on the quantile regression of scores rather than density estimation.

Most relevant to our work is the approach of performing quantile regression directly on conformity scores [Gibbs et al. \[2025a\]](#), [Kiyani et al. \[2024\]](#), [Plassier et al. \[2025a\]](#). As aforementioned, the excess risk of the pinball loss constitutes an upper bound on the MSCE. Specifically, [Plassier et al. \[2025a\]](#) propose a general framework called Rectified Conformal Prediction (RCP), which transforms the original nonconformity score into a rectified version that tries to remove the covariate-dependent part in the score and thereby naturally improves conditional coverage of standard split conformal prediction with these rectified scores. However, naive quantile regression with the pinball loss faces intrinsic limitations, even for marginal coverage in high-dimensional settings [Gibbs et al. \[2025b\]](#). In our context, we identify that naive quantile regression overlooks a critical heteroscedastic component. Our method aims to recover this missing component, yielding a significantly sharper approximation to the MSCE.

2 Preliminaries

Split Conformal Prediction. We consider the standard setting where we observe data points $(X, Y) \in \mathcal{X} \times \mathcal{Y}$ drawn i.i.d. from an unknown joint distribution P_{XY} . In the split conformal prediction framework [Papadopoulos et al. \[2002\]](#), the available data is randomly partitioned into two disjoint subsets: a proper training set $\mathcal{D}_{\text{train}}$ and a calibration set $\mathcal{D}_{\text{cal}} = \{(X_i, Y_i)\}_{i=1}^n$ of size n . A predictive model is first fitted on $\mathcal{D}_{\text{train}}$. We then define a nonconformity score function $S : \mathcal{X} \times \mathcal{Y} \rightarrow \mathbb{R}$, which measures the discrepancy between the target y and the model's prediction at x (e.g., the absolute residual $S(x, y) = |y - \hat{\mu}(x)|$). The scores are computed for all calibration points as $s_i = S(X_i, Y_i)$ for all $i \in \{1, \dots, n\}$. Given a user-specified miscoverage level $\alpha \in (0, 1)$, we compute the conformal threshold \hat{q} as the $\lceil (n+1)(1-\alpha) \rceil / n$ -th empirical quantile of the calibration scores $\{s_1, \dots, s_n\}$. For a new test input X_{n+1} , the prediction set is constructed as $\mathcal{C}(X_{n+1}) = \{y \in \mathcal{Y} : S(X_{n+1}, y) \leq \hat{q}\}$. This procedure satisfies the finite-sample marginal coverage guarantee:

$$1 - \alpha \leq \mathbb{P}(Y_{n+1} \in \mathcal{C}(X_{n+1})) \leq 1 - \alpha + \frac{1}{n+1}. \quad (1)$$

Rectified Conformal Prediction (RCP). As has been widely noted, the failure pattern of standard split conformal prediction is under-coverage in hard regions and over-coverage in easy ones. To improve the conditional coverage, [Plassier et al. \[2025a\]](#) propose RCP, which transforms the raw nonconformity scores into a rectified version that is approximately homoscedastic. While the RCP framework allows for general transformations, we focus on the fundamental additive correction in our work.

Specifically, let $\hat{q}_{1-\alpha} : \mathcal{X} \rightarrow \mathbb{R}$ be an estimator of the conditional $(1 - \alpha)$ -quantile of the raw score $S(X, Y)$ given X . The rectified score function $R : \mathcal{X} \times \mathcal{Y} \rightarrow \mathbb{R}$ is defined as the deviation from this estimated quantile:

$$R(x, y) := S(x, y) - \hat{q}_{1-\alpha}(x). \quad (2)$$

The conformal procedure is then applied to these rectified scores. We compute the rectified scores on the calibration set, $\mathcal{R}_{\text{cal}} = \{R(x_i, y_i)\}_{i=1}^n$, and find their $\lceil (n+1)(1-\alpha) \rceil / n$ -th empirical quantile, denoted by $\hat{\gamma}$. The resulting prediction set for a new test point X_{n+1} is constructed as:

$$\mathcal{C}(X_{n+1}) = \{y \in \mathcal{Y} : S(X_{n+1}, y) \leq \hat{q}_{1-\alpha}(X_{n+1}) + \hat{\gamma}\}. \quad (3)$$

Intuitively, $\hat{q}_{1-\alpha}(x)$ serves as a coarse, instance-dependent baseline threshold, while $\hat{\gamma}$ acts as a global, residual correction to ensure exact marginal validity.

Conditional coverage. Given marginal validity, our primary concern is the *conditional coverage*, defined as:

$$\pi(x) := \mathbb{P}(Y \in \mathcal{C}_\alpha(X) \mid X = x), \quad (4)$$

which characterizes the coverage probability for each specific instance x . Rather than considering any relaxed form, we focus on controlling the exact conditional coverage.

Since $\pi(x)$ is a function of x , a natural approach is to construct a metric that summarizes its deviation from the target level $1 - \alpha$. Following [Kiyani et al. \[2024\]](#), we define the Mean Squared Conditional Error (MSCE) as:

$$\text{MSCE} := \mathbb{E}[(\pi(X) - (1 - \alpha))^2]. \quad (5)$$

We further motivate this metric through a novel lens. Viewing $\pi(X)$ as a random variable, the tower property implies that its expectation is the marginal coverage:

$$\mathbb{E}[\pi(X)] = \mathbb{P}(Y \in \mathcal{C}_\alpha(X)), \quad (6)$$

which is controlled due to marginal validity as stated in Equation 1. Given this, achieving conditional validity reduces to establishing concentration of $\pi(X)$, which naturally amounts to controlling its variance. Marginal validity ensures that $\mathbb{E}[\pi(X)]$ converges to the target level $1 - \alpha$ at the fast rate $O(n^{-1})$; consequently, the bias term is negligible, and the variance is nearly equivalent to the MSCE.

Quantile regression. Our framework relies on estimating the conditional quantiles of the nonconformity scores. Formally, let $Z \in \mathbb{R}$ be a target random variable (typically the score S in our context) and $X \in \mathcal{X}$ be the covariates. We denote the true conditional τ -th quantile of Z given $X = x$ as $q_\tau(x) := \inf\{z : \mathbb{P}(Z \leq z \mid X = x) \geq \tau\}$ for a level $\tau \in (0, 1)$. Standard quantile regression estimates q_τ by minimizing the expected pinball loss [Koenker \[2005\]](#). The pinball loss function $\rho_\tau : \mathbb{R} \times \mathbb{R} \rightarrow \mathbb{R}_{\geq 0}$ is defined as:

$$\rho_\tau(q, u) := \max\{\tau(u - q), (\tau - 1)(u - q)\}. \quad (7)$$

In practice, given a hypothesis class \mathcal{G} (e.g., neural networks), we seek an estimator $\hat{g} \in \mathcal{G}$ that minimizes the empirical risk $\frac{1}{n} \sum_{i=1}^n \rho_\tau(z_i, g(x_i))$. A fundamental property of this objective is that, assuming sufficient model capacity, the population minimizer $g^* := \arg \min_g \mathbb{E}[\rho_\tau(Z, g(X))]$ uniquely recovers the true conditional quantile q_τ .

3 Approximation to MSCE

In general, without a generative model, we typically observe only a single realization of Y for each instance X . As a result, although the MSCE is a theoretically well-motivated metric, it is inherently difficult to

evaluate—and hence to optimize—in practice. To address this challenge, Kiyani et al. [2024] derived an upper bound on the MSCE, while Plassier et al. [2025a] established a stronger pointwise bound on the deviation $|F_{S|X}(\hat{q}_{1-\alpha}(x)) - (1 - \alpha)|$. Though there is a gap between $F_{S|X}(\hat{q}_\tau(x))$ and $\pi(x)$ in RCP due to the conformalization step after quantile regression, Plassier et al. [2025a] proves that it shrinks at an exponential rate w.r.t. the size of sample used for conformalization.

Hereafter, we will use $\tau := 1 - \alpha$ to denote the target coverage level, and $\hat{q}_\tau(x)$ to denote the estimated conditional τ -quantile of the nonconformity scores. We now introduce the pointwise results that motivate quantile regression with standard pinball loss Plassier et al. [2025a].

Proposition 3.1. *Assume the conditional CDF of scores is L_F -Lipschitz, under mild regularity conditions,*

$$|F_{S|X}(\hat{q}_\tau(x)) - \tau| \leq \sqrt{2L_F(\mathcal{L}_x(\hat{q}_\tau(x)) - \mathcal{L}_x(q_\tau(x)))} \quad (8)$$

holds. Here, $\mathcal{L}_x(\cdot) = \mathbb{E}_Y[\rho_\tau(\cdot, s(x, Y))]$ denotes the expected pinball loss (with expectation taken over $Y | X$).

The proof is detailed in Appendix B.1. Next, we introduce the assumption on consistency of quantile estimators and our approximation for the MSCE based on Taylor expansion.

Assumption 3.2. We assume the quantile estimator \hat{q}_τ is L_2 -consistent, i.e., $\epsilon_q(x) := \hat{q}_\tau(x) - q_\tau(x)$ satisfies:

$$\|\epsilon_q\|_{L_2(\mathbb{P}_X)} \xrightarrow{p} 0 \quad \text{as } n \rightarrow \infty \quad (9)$$

Remark 3.3. Assumption 3.2 only requires L_2 -consistency to demonstrate the leading term in Proposition 3.4. In later sections, when analyzing the finite-sample performance, we establish a fast convergence rate for \hat{q}_τ .

We then define the Mean Squared Quantile Error (MSQE) as the first step to derive a tractable surrogate of MSCE.

$$\text{MSQE}(\hat{q}_\tau) := \mathbb{E}_X \left[(F_{S|X}(\hat{q}_\tau(x)) - \tau)^2 \right]. \quad (10)$$

Next, to circumvent estimating the full conditional distribution $F_{S|X}$, we fix \hat{q}_τ at q_τ , which constitutes the key step toward tractability. This is achieved via Taylor expansions, as formalized in the following proposition.

Proposition 3.4. *Let $G(u) := (F_{S|X}(u) - \tau)^2$, and let $\mathcal{E}(x) := \mathcal{L}_x(\hat{q}_\tau(x)) - \mathcal{L}_x(q_\tau(x))$ denotes the pointwise excess risk with pinball loss. We have following two Taylor expansions with Lagrange remainder:*

$$G(\hat{q}_\tau(x)) = f_{S|X}(q_\tau(x))^2 \epsilon_q(x)^2 + \frac{1}{6} G'''(\xi_{S,1}) \epsilon_q(x)^3, \quad (11)$$

and

$$\mathcal{E}(x) = f_{S|X}(q_\tau(x)) \epsilon_q(x)^2 + \frac{1}{6} f'_{S|X}(\xi_{S,2}) \epsilon_q(x)^3, \quad (12)$$

where $\xi_{S,1}$ and $\xi_{S,2}$ both lie between $\hat{q}_\tau(x)$ and $q_\tau(x)$.

Under Assumption 3.2 and mild regularity conditions on the density $f_{S|X}$, the squared conditional quantile error admits the following expansion:

$$(F_{S|X}(\hat{q}_\tau(x)) - \tau)^2 = 2f_{S|X}(q_\tau(x))\mathcal{E}(x) + C_f \epsilon_q(x)^3, \quad (13)$$

where C_f is a constant that characterizes the smoothness of $f_{S|X}$. Consequently, the MSQE satisfies:

$$\text{MSQE} = 2\mathbb{E}_X[f_{S|X}(q_\tau(X))\mathcal{E}(X)] + C_f \mathbb{E}_X[\epsilon_q(X)^3], \quad (14)$$

and the first term serves as our final optimization surrogate.

The proof of Proposition 3.4 is provided in Appendix B.2. Now we delineate the implications of Proposition 3.4: rather than minimizing the risk with plain pinball loss, our approximation motivates a weighted version. The oracle weight is $f_{S|X}(q_\tau(x))$, i.e., the conditional density of scores evaluated at the true quantile. To provide intuitions of this density weight, we consider the location-scale family as an example.

Example 3.1. Consider the case where the nonconformity score S given X follows a location-scale family:

$$S = \nu(x) + \sigma(x)\xi, \quad (15)$$

where ξ is a standardized random variable with a base PDF $f_0(\cdot)$ (e.g., standard normal or Laplace) and CDF $F_0(\cdot)$. The conditional density of S is given by $f_{S|X}(s) = \frac{1}{\sigma(x)} f_0\left(\frac{s-\nu(x)}{\sigma(x)}\right)$. Let $z_\tau = F_0^{-1}(\tau)$ be the τ -quantile of the base distribution. The true conditional quantile of the score is then $q_\tau(x) = \nu(x) + \sigma(x)z_\tau$. Evaluating the conditional density at the true quantile yields:

$$f_{S|X}(q_\tau(x)) = \frac{1}{\sigma(x)} f_0(z_\tau) \propto \frac{1}{\sigma(x)}. \quad (16)$$

This example shows that minimizing the standard pinball loss collapses the spectrum of heteroscedasticity inherent in the MSQE objective into a single, unweighted error criterion. Motivated by the need to recover this heteroscedastic spectrum, we refer to our approach as colorful pinball, in contrast to the conventional plain pinball loss.

The severity of this objective misalignment depends on the degree of heteroscedasticity in the scores (and intrinsically, in $Y | X$). We note that the quantile has characterized heteroscedasticity, yet our approximation reveals that **more stress on heteroscedasticity** is needed when targeting conditional coverage. To see this, recall Equation (11) and (12). Therefore, although minimizing either the standard or density-weighted pinball loss recovers the true quantile asymptotically, a severe misalignment persists with finite samples, which is precisely what we do correctly.

Remark 3.5. In Example 3.1, the weight $1/\sigma(x)$ may appear counterintuitive as it assigns lower importance to high-variance regions. However, we note that this weight is put on the distance of two quantiles, and a small $\sigma(x)$ corresponds to a steeper $F_{S|X}$, making the coverage probability highly sensitive to estimation errors; a slight deviation in $\hat{q}_\tau(x)$ can drastically degrade coverage (e.g., from 95% to 80%). Thus, normalizing by $\sigma(x)$ effectively standardizes this sensitivity across instances, promoting a stable coverage independent of x , i.e., $\pi(x) \approx \text{const}$.

4 Colorful Pinball Conformal Prediction

4.1 Algorithm details

Figure 1 illustrates the proposed workflow. We begin by partitioning the calibration set \mathcal{D}_{cal} into three disjoint subsets: $\mathcal{D}_{\text{cal},1}$, $\mathcal{D}_{\text{cal},2}$, and $\mathcal{D}_{\text{cal},3}$. Our objective targets the leading term in Equation (14), which can be reformulated as:

$$\mathbb{E}_X[f_{S|X}(q_\tau(X))\mathcal{E}(X)] = \mathbb{E}_{X,Y} [f_{S|X}(q_\tau(X))\rho_\tau(\hat{q}_\tau(X), S(X, Y))] \quad (17)$$

To optimize this empirically, we require an estimate of the weight $w(x) := f_{S|X}(q_\tau(X))$. Instead of estimating the full conditional density $f_{S|X}$, we note that the quantile function is the inverse function of the CDF. Thus,

we have:

$$\frac{\partial q_\tau(x)}{\partial \tau} = \frac{1}{f_{S|X}(q_\tau(x))}. \quad (18)$$

Consequently, we approximate the density weight using the finite-difference estimator:

$$\hat{w}(x) = \frac{2\delta}{\hat{q}_{\tau+\delta}(x) - \hat{q}_{\tau-\delta}(x)}. \quad (19)$$

This offers a clear benefit: it requires estimating only two auxiliary quantiles, $q_{\tau+\delta}(x)$ and $q_{\tau-\delta}(x)$, alongside the primary target $q_\tau(x)$. This structure naturally motivates a multitask learning framework. We employ a shared feature extractor $h(x)$ coupled with three distinct output heads:

$$\begin{aligned} \hat{q}_\tau(x) &= \phi_{\text{main}} \circ h(x) \\ \hat{q}_{\tau+\delta}(x) &= \hat{q}_\tau(x) + \text{Softplus}(\phi_{\text{high}} \circ h(x)) \\ \hat{q}_{\tau-\delta}(x) &= \hat{q}_\tau(x) - \text{Softplus}(\phi_{\text{low}} \circ h(x)). \end{aligned} \quad (20)$$

Here, the $\text{Softplus}(\cdot) = \log(1 + \exp(\cdot))$ activation is employed to ensure monotonicity, preventing quantile crossing that would otherwise yield invalid negative weights w_i . In practice, h and the projection heads $\{\phi\}$ are parameterized by neural networks (e.g., MLPs).

We observe that the approximation error derived from the Taylor expansion in Equation (14) is contingent on the accuracy of the quantile estimates. Therefore, we first perform joint training of all three estimators on $\mathcal{D}_{\text{cal},1}$ using the standard plain pinball loss. With this initialization, we freeze the backbone h and fine-tune the primary head ϕ_{main} on $\mathcal{D}_{\text{cal},2}$:

$$\phi_{\text{main}} = \underset{\phi}{\operatorname{argmin}} \sum_{i \in \mathcal{D}_{\text{cal},2}} \hat{w}(x_i) \rho_\tau(\phi \circ h(x_i), s_i). \quad (21)$$

The resulting quantile estimator is the final version: $\hat{q}_\tau = \phi_{\text{main}} \circ h$. To ensure marginal validity, we apply RCP by computing the residuals on $\mathcal{D}_{\text{cal},3}$:

$$R_j = S_j - \hat{q}_\tau(x_j). \quad (22)$$

We then compute $\hat{\gamma}$ as the $\lceil (|\mathcal{D}_{\text{cal},3}| + 1)(\tau) \rceil$ -th smallest value of $\{R_j\}_{j \in \mathcal{D}_{\text{cal},3}}$ and construct the conformal set:

$$\mathcal{C}_\alpha(x_{\text{test}}) = \{y : S(x_{\text{test}}, y) \leq \hat{\gamma} + \hat{q}_\tau(x_{\text{test}})\}. \quad (23)$$

For instance, the classic absolute residual score $S(x, y) = |y - \hat{\mu}(x)|$ for scalar regression yields:

$$\mathcal{C}_\alpha(x_{\text{test}}) = [\hat{\mu}(x_{\text{test}}) \pm (\hat{q}_\tau(x_{\text{test}}) + \hat{\gamma})]. \quad (24)$$

The complete procedure is summarized in Algorithm 1.

4.2 Towards better finite-sample stability

We now introduce supplementary mechanisms to enhance the empirical stability of our methodology. As defined in Equation (19), the proposed estimator relies on inverse weighting, where the denominator corresponds to the estimated inter-quantile gap $\hat{q}_{\tau+\delta}(x_i) - \hat{q}_{\tau-\delta}(x_i)$. A vanishing denominator—often caused by

Algorithm 1 Colorful Pinball Conformal Prediction

- 1: **Input:** Calibration data \mathcal{D}_{cal} , Point predictor $\hat{\mu}$, Test input x_{test} , Target coverage level τ , Bandwidth δ
- 2: Split \mathcal{D}_{cal} into three disjoint parts $\mathcal{D}_{\text{cal},1}, \mathcal{D}_{\text{cal},2}, \mathcal{D}_{\text{cal},3}$.
- 3: Compute conformity scores S_i for all $(x_i, y_i) \in \mathcal{D}_{\text{cal}}$.
- 4: Train three quantile estimators $\hat{q}_{\text{low}}, \hat{q}_{\text{main}}$, and \hat{q}_{high} (for levels $\tau - \delta, \tau, \tau + \delta$) jointly on $\mathcal{D}_{\text{cal},1}$.
- 5: Compute the weight for all $(x_i, y_i) \in \mathcal{D}_{\text{cal},2}$:

$$w_i \leftarrow \frac{2\delta}{\hat{q}_{\text{high}}(x_i) - \hat{q}_{\text{low}}(x_i)}.$$

- 6: Fine-tune the parameters of \hat{q}_{main} on $\mathcal{D}_{\text{cal},2}$ to get the final quantile estimator \hat{q}_τ .
- 7: Compute residuals for all $(x_j, y_j) \in \mathcal{D}_{\text{cal},3}$:

$$R_j \leftarrow S_j - \hat{q}_\tau(x_j)$$

- 8: Compute empirical quantile $\hat{\gamma}$ as the $\lceil (|\mathcal{D}_{\text{cal},3}| + 1)\tau \rceil$ -th smallest value of $\{R_j\}$.
- 9: **Output:** $\mathcal{C}_\alpha(x_{\text{test}}) = \{y : S(x_{\text{test}}, y) \leq \hat{\gamma} + \hat{q}_\tau(x_{\text{test}})\}$

estimation errors—can yield arbitrarily large weights w_i , leading to explosive variance in the optimization objective. Theoretically, ensuring stability requires the sample size n to be sufficiently large for the neural network to reliably distinguish the $(\tau - \delta)$ and $(\tau + \delta)$ quantiles (e.g., 89% vs. 91%), thereby keeping the estimated gap bounded away from zero.

To stabilize the fine-tuning procedures, particularly in regimes where the bandwidth δ is small relative to n , we propose two strategies: *weight clipping* and *loss mixing*.

- **Weight Clipping:** We truncate excessive weights to a threshold. This threshold can be set as a multiple M of the empirical mean of the weights.
- **Loss Mixing:** We modify the optimization objective as a convex combination of the normalized weighted pinball loss and the plain pinball loss.

In essence, these two strategies correspond to imposing artificial upper and lower bounds on the estimated weights, a modification motivated by the theoretical bottlenecks identified in the proof of our main theorem (Theorem 5.2). Furthermore, such clipping strategies are widely recognized as effective in settings involving reciprocal weighting; they significantly reduce variance at the cost of introducing slight bias, a trade-off commonly utilized in policy evaluation (e.g., clipping inverse propensity weights; [Swaminathan and Joachims, 2015](#)). We demonstrate the empirical benefits of these strategies in Section 6 and Appendix A.

5 Theoretical Analysis

To approximate MSCE, i.e., the MSE of coverage probability $\pi(x)$, we employ a two-step transformation. First, we substitute the target $\pi(x)$ with $F_{S|X}(\hat{q}_\tau(x))$; second, we select the leading term derived in Proposition 3.4 as our final optimization surrogate. According to Algorithm 1, the first substitution introduces a discrepancy due to the global conformal shift $\hat{\gamma}$ required for marginal coverage. However, as shown by [Plassier et al.](#)

[2025a], this gap decays exponentially with the calibration sample size m^1 , provided \hat{q}_τ satisfies certain regularity conditions that controls the quality of quantile estimator \hat{q}_τ (see Appendix C.1). Intuitively, with a moderately large sample size of $\mathcal{D}_{\text{calib}}$ (e.g., in the hundreds), we can focus on characterizing the finite-sample performance of our method through analyzing the MSE of $F_{S|X}(\hat{q}_\tau(x))$, and naturally the surrogate, expected risk of density-weighted pinball loss.

We now present our main technical assumptions as follows.

Assumption 5.1. Let $\mathcal{X} \subset \mathbb{R}^d$ be compact, we assume:

1. **Quantile smoothness in τ .** The conditional quantile function $q_\tau(x)$ is three times continuously differentiable with respect to τ for all $x \in \mathcal{X}$, and

$$\sup_{x \in \mathcal{X}} \left| \frac{\partial^3 q_\tau(x)}{\partial \tau^3} \right| \leq B_q'''.$$

2. **Density regularity at the target quantile.** There exist constants b_w, B_w such that:

$$0 < b_w \leq f_{S|X}(q_\tau(x) \mid x) \leq B_w < \infty, \quad \forall x \in \mathcal{X},$$

3. **Local Hölder-type norm equivalence.** There exist constants $C_{\text{norm}} > 0$, $\nu \in (0, 1]$, and $r > 0$ such that for all $g \in \mathcal{G}$ satisfying $\|g - g^*\|_{L_2(\mathbb{P}_X)} \leq r$,

$$\|g - g^*\|_{L_\infty(\mathcal{X})} \leq C_{\text{norm}} \|g - g^*\|_{L_2(\mathbb{P}_X)}^\nu.$$

Among these assumptions, the first two are standard technical conditions, whereas the third is less conventional and warrants a more detailed discussion due to its pivotal role in our proof. The primary challenge in bounding the generalization error of our method stems from the estimated reciprocal weights: specifically, we require a pointwise lower bound on the denominator, whereas typical guarantees yield only L_2 convergence. To bridge this gap, we introduce this norm-equivalence assumption, which we relax to hold only locally within a neighborhood of the true quantile function g^* . In general, it suffices that $g - g^*$ belongs to a Hölder class for this assumption to hold. We provide a proof of this claim in Appendix B.4, which can also be obtained as a special case of the celebrated Gagliardo–Nirenberg interpolation inequality. Finally, we note that the exponent ν increases with the smoothness of the function class; for instance, $\nu = 1$ for parametric models or regression in a Reproducing Kernel Hilbert Space with a smooth kernel (e.g., Gaussian or Laplacian).

We then introduce the necessary definitions for presenting the main theorem. Let \mathcal{G} be a hypothesis class with empirical Rademacher complexity $\mathfrak{R}_n(\mathcal{G})$. Let $\mathcal{R}(g) = \mathbb{E}_X[w(X)\rho_\tau(g(X), S)]$ be the expected risk of weighted pinball loss. Let the weights be estimated by $\hat{w}(x) = 2\delta/(\hat{q}_{\tau+\delta}(x) - \hat{q}_{\tau-\delta}(x))$ where the two $\hat{q}_\beta \in \mathcal{G}$ are the auxiliary quantile estimators derived through empirical risk minimization (ERM) with standard pinball loss. Let $\mathcal{E}_q(n) := \sup_{\beta \in \{\tau-\delta, \tau+\delta\}} \|\hat{q}_\beta - q_\beta\|_{L_2(\mathbb{P}_X)}$ denote the estimation error of two auxiliary quantiles. Finally, let $M_{\rho, \mathcal{G}} := \sup_{g \in \mathcal{G}} (\mathbb{E}_n[\rho_\tau(g(X), S)^2])^{1/2}$, and let σ_S denote the bound on conditional sub-Gaussian scale of scores.

Theorem 5.2. Under Assumption 5.1, with probability at least $1 - 3\zeta$, setting the finite-difference bandwidth to $\delta^* \asymp (\mathfrak{R}_n(\mathcal{G}))^{1/3}$, with appropriately large n , the excess risk satisfies:

$$\mathcal{R}(\hat{g}) - \mathcal{R}(g^*) = O\left(\mathfrak{R}_n(\mathcal{G})^{\frac{2}{3}}\right), \quad (25)$$

¹We denote $|\mathcal{D}_{\text{calib},3}| = m$ and $|\mathcal{D}_{\text{calib},1}| = |\mathcal{D}_{\text{calib},2}| = n$.

which is of $O(n^{-1/3})$ with fast rate established by local Rademacher complexity.

Specifically, the exact non-asymptotic bound is given by:

$$\begin{aligned} \mathcal{R}(\hat{g}) - \mathcal{R}(g^*) &\leq C_1 \mathfrak{R}_n(\mathcal{G}) + C_2 \sqrt{\frac{\log(1/\zeta)}{n}} \\ &\quad + C_3 \left(\mathcal{E}_q(n)^2 + C_4 \mathcal{E}_q(n)^{1+\nu} \sqrt{\frac{\log(1/\zeta)}{n}} \right. \\ &\quad \left. + C_5 \frac{\mathcal{E}_q(n)^{2\nu} \log(1/\zeta)}{n} \right)^{1/3}, \end{aligned} \quad (26)$$

where constants $C_1 = 4B_w L_\rho$, $C_2 = 2\sqrt{2}B_w L_\rho \sigma_S$, $C_3 = 2^{5/3}3^{2/3}M_{\rho,\mathcal{G}}B_w^2(B_q''')^{1/3}$, $C_4 = 2^{\nu+1/2}C_{\text{norm}}$, $C_5 = C_{\text{norm}}^2/3$, $L_\rho = \max\{\tau, 1-\tau\}$.

In the asymptotic regime, there is a rate loss due to weight estimation, compared to the direct quantile regression for q_τ with plain pinball loss. Compared to direct quantile regression with the pinball loss, our method exhibits a slower asymptotic rate due to the additional error introduced by estimating density-based weights. However, we emphasize that the primary value of conformal prediction lies in the finite-sample regime, which motivates the exact non-asymptotic expression in our theory. In finite samples, although direct quantile regression may converge faster, the misalignment of its optimization objective with conditional coverage can substantially limit its performance, as illustrated in Proposition 3.4 and Example 3.1. On the other hand, when higher-order central finite-difference schemes of order k are employed [Fornberg \[1988\]](#), the resulting excess risk rate can be further improved to $O(\mathfrak{R}_n(\mathcal{G})^{2k/(2k+1)})$.

Table 1: Comparison of MSCE. Mean Squared Coverage Error (MSCE, ↓) on 8 high-dimensional benchmarks. Best results are **bolded**.

Method	Bike	Diamond	Gas Turbine	Naval	SGEMM	Superconductivity	Transcoding	WEC
Split	0.0030 ± 0.0007	0.0127 ± 0.0029	0.0033 ± 0.0007	0.0349 ± 0.0120	0.0035 ± 0.0009	0.0073 ± 0.0008	0.0045 ± 0.0019	0.0123 ± 0.0017
PLCP	0.0018 ± 0.0007	0.0022 ± 0.0027	0.0008 ± 0.0008	0.0172 ± 0.0100	0.0028 ± 0.0014	0.0014 ± 0.0007	0.0034 ± 0.0026	0.0016 ± 0.0012
Gaussian-Scoring	0.0010 ± 0.0005	0.0006 ± 0.0004	0.0005 ± 0.0002	0.0169 ± 0.0136	0.0021 ± 0.0028	0.0031 ± 0.0013	0.0020 ± 0.0019	0.0071 ± 0.0018
CQR	0.0015 ± 0.0010	0.0026 ± 0.0010	0.0006 ± 0.0004	0.0207 ± 0.0079	0.0013 ± 0.0005	0.0011 ± 0.0008	0.0013 ± 0.0013	0.0068 ± 0.0009
CQR-ALD	0.0012 ± 0.0010	0.0013 ± 0.0005	0.0006 ± 0.0003	0.0170 ± 0.0112	0.0010 ± 0.0005	0.0009 ± 0.0006	0.0010 ± 0.0005	0.0046 ± 0.0013
RPC	0.0016 ± 0.0005	0.0033 ± 0.0008	0.0006 ± 0.0003	0.0048 ± 0.0034	0.0013 ± 0.0003	0.0017 ± 0.0005	0.0009 ± 0.0005	0.0039 ± 0.0007
RPC-ALD	0.0010 ± 0.0004	0.0019 ± 0.0008	0.0004 ± 0.0002	0.0089 ± 0.0066	0.0011 ± 0.0004	0.0011 ± 0.0006	0.0007 ± 0.0003	0.0031 ± 0.0006
CPCP	0.0011 ± 0.0006	0.0006 ± 0.0003	0.0005 ± 0.0002	0.0020 ± 0.0011	0.0003 ± 0.0002	0.0008 ± 0.0004	0.0010 ± 0.0006	0.0015 ± 0.0005
CPCP (Clip+Mix)	0.0008 ± 0.0003	0.0004 ± 0.0002	0.0003 ± 0.0001	0.0017 ± 0.0008	0.0003 ± 0.0001	0.0007 ± 0.0004	0.0003 ± 0.0001	0.0010 ± 0.0003

6 Experiments

In this section, we present extensive experiments across eight classic datasets to validate our methodology. Due to limited space, we leave the details of the data description and detailed experimental results in [Appendix A](#).

Data. In summary, we consider eight real-world regression benchmarks spanning engineering systems, energy, transportation, and economics. Most of them are from the classic UCI repository [Kelly et al. \[2025\]](#). Among them, three datasets (Bike, Diamond, and Superconductivity) have one-dimensional responses, while

Table 2: Comparison of WSC. Worst-Slice Coverage (WSC, \uparrow) on 8 high-dimensional benchmarks. Best results are **bolded**.

Method	Bike	Diamond	Gas Turbine	Naval	SGEMM	Superconductivity	Transcoding	WEC
Split	0.8083 ± 0.0265	0.6492 ± 0.0180	0.8134 ± 0.0183	0.5703 ± 0.0574	0.7470 ± 0.0097	0.7824 ± 0.0237	0.7239 ± 0.0194	0.7462 ± 0.0165
PLCP	0.8534 ± 0.0242	0.8286 ± 0.0585	0.8711 ± 0.0218	0.6821 ± 0.0925	0.7803 ± 0.0441	0.8661 ± 0.0218	0.7936 ± 0.0499	0.8630 ± 0.0198
Gaussian-Scoring	0.8605 ± 0.0319	0.8607 ± 0.0140	0.8727 ± 0.0180	0.6723 ± 0.0870	0.8251 ± 0.0530	0.8314 ± 0.0239	0.8287 ± 0.0356	0.8017 ± 0.0224
CQR	0.8653 ± 0.0296	0.8162 ± 0.0166	0.8752 ± 0.0170	0.6440 ± 0.0560	0.8284 ± 0.0268	0.8682 ± 0.0224	0.8313 ± 0.0204	0.8050 ± 0.0162
CQR-ALD	0.8699 ± 0.0265	0.8457 ± 0.0148	0.8750 ± 0.0177	0.6724 ± 0.0708	0.8462 ± 0.0212	0.8753 ± 0.0196	0.8378 ± 0.0250	0.8121 ± 0.0195
RCP	0.8662 ± 0.0285	0.7952 ± 0.0155	0.8780 ± 0.0198	0.7963 ± 0.0546	0.8291 ± 0.0155	0.8572 ± 0.0223	0.8272 ± 0.0168	0.8318 ± 0.0117
RCP-ALD	0.8722 ± 0.0210	0.8310 ± 0.0173	0.8860 ± 0.0125	0.7459 ± 0.0827	0.8360 ± 0.0164	0.8709 ± 0.0217	0.8570 ± 0.0142	0.8428 ± 0.0139
CPCP	0.8757 ± 0.0189	0.8685 ± 0.0173	0.8824 ± 0.0180	0.8323 ± 0.0374	0.8886 ± 0.0145	0.8618 ± 0.0205	0.8599 ± 0.0135	0.8518 ± 0.0192
CPCP (Clip+Mix)	0.8932 ± 0.0142	0.8772 ± 0.0136	0.8857 ± 0.0126	0.8346 ± 0.0345	0.8833 ± 0.0138	0.8790 ± 0.0196	0.8805 ± 0.0124	0.8692 ± 0.0143

the remaining five involve multi-dimensional responses. The covariate dimension ranges from a moderate scale (tens of features), and the sample size varies between 10k and 50k. Each dataset is randomly split into training, calibration, and test sets with an approximate ratio of 6:2:2.

Baselines. We consider standard baselines including Split Conformal Prediction (Split; [Papadopoulos et al., 2002](#)), Partition Learning Conformal Prediction (PLCP; [Kiyani et al., 2024](#)), Gaussian Scoring [Braun et al. \[2025a\]](#), CQR [Romano et al. \[2019\]](#), RCP [Plassier et al. \[2025a\]](#). In addition, to separately validate the value of our approximation described in Proposition 3.4, we select a parametric likelihood on nonconformity score, the Asymmetric Laplace Distribution (ALD), of which the maximum likelihood estimation (MLE) is equivalent to minimizing scaled pinball loss and a regularization term on scales $\sigma(x)$. We construct two baselines based on CQR and RCP through substituting the quantile regression with MLE of ALD, which does not involve the rectification procedures. We provide the details of baselines in Appendix A.2.

Except for Gaussian Scoring, we adopt l_∞ norm of residuals as nonconformity scores [Diquigiovanni et al. \[2024\]](#), which reduces to the standard absolute residual score for the case of one-dimensional labels.

Metrics. To approximately evaluate the conditional coverage in real-world datasets, where we have no access to the data generation mechanism, we adopt clustering (K-means; [Braun et al., 2025b](#)) for MSCE and random projection for Worst-Slice Coverage (WSC; [Cauchois et al., 2021, Romano et al., 2020](#)). In general, given marginal validity, both lower MSCE and higher WSC imply better concentration of conditional coverage probabilities, and WSC is additionally a robustness measure that characterizes the worst-case coverage. Throughout the experiments, we set the target coverage level $\tau = 90\%$. We also report the mean (per dimension) of the log volume of the predictive set to characterize the efficiency. All methods are run with 20 Monte Carlo repetitions to evaluate the metrics, and we report mean \pm std. The details of metrics are provided in Appendix A.4.

6.1 Results analysis

We present the main part of results in Table 1 and 2, and all results with ablation studies can be found in Appendix A.5. In summary, our methodology achieves impressive improvement on conditional coverage across all benchmarks, with a medium predictive set size among all baselines (per set size, see Table 6). Specifically, the improvement on WSC is remarkable, which would be more pronounced if considering $(\tau - \text{WSC})$, i.e, the worst-case miscoverage probability. In addition, we observe that the advantage of our

methods becomes more prominent when standard Split CP performs badly, e.g., on Diamond and Naval, which corresponds to a more challenging setting. Moreover, we find that the parametric likelihood (ALD) indeed brings benefits in most cases, which further validates our approximation. Finally, our two additional mechanisms for stability work very well, as also further demonstrated in Table 4 and 5.

Overall, these results empirically corroborate our claim: although density-weighted optimization introduces additional estimation error, it consistently yields superior conditional coverage in the finite-sample regime, where objective misalignment dominates asymptotic considerations.

7 Conclusion

In this paper, we investigate the problem of improving conditional coverage in conformal prediction with finite samples and black-box predictors. By analyzing the MSE of conditional coverage probabilities, we identify a fundamental limitation in a ubiquitous component of conformal procedures: standard quantile regression with pinball loss. We note that while the conformalization step effectively addresses coverage bias, reducing variance necessitates a mechanism that precisely captures heteroscedasticity. To this end, we develop a Taylor-based approximation that accurately recovers the underlying heteroscedastic structure in the MSE. Building on this insight, we propose a principled algorithmic framework with exact non-asymptotic excess risk guarantees. Extensive experiments demonstrate the superior performance of our methodology, with ablation studies further validating the contribution of each component.

We emphasize that the primary value of conformal prediction lies in the finite-sample regime, and accordingly adopt a restrained modeling strategy by employing joint quantile regression rather than explicit density estimation on the calibration set. We hope our results provide useful insights for the design of practical conformal prediction procedures.

References

Anastasios N Angelopoulos, Rina Foygel Barber, and Stephen Bates. Theoretical foundations of conformal prediction. *arXiv preprint arXiv:2411.11824*, 2024.

Francis Bach. *Learning theory from first principles*. MIT press, 2024.

Peter L Bartlett, Olivier Bousquet, and Shahar Mendelson. Local rademacher complexities. *The Annals of Statistics*, 33(4):1497–1537, 2005.

Michael Bian and Rina Foygel Barber. Training-conditional coverage for distribution-free predictive inference. *Electronic Journal of Statistics*, 17(2):2044–2066, 2023.

Sacha Braun, Eugène Berta, Michael I Jordan, and Francis Bach. Multivariate conformal prediction via conformalized gaussian scoring. *arXiv preprint arXiv:2507.20941*, 2025a.

Sacha Braun, David Holzmüller, Michael I. Jordan, and Francis Bach. Conditional coverage diagnostics for conformal prediction, 2025b.

Maxime Cauchois, Suyash Gupta, and John C Duchi. Knowing what you know: valid and validated confidence sets in multiclass and multilabel prediction. *Journal of machine learning research*, 22(81):1–42, 2021.

Tiffany Ding, Anastasios Angelopoulos, Stephen Bates, Michael Jordan, and Ryan J Tibshirani. Class-conditional conformal prediction with many classes. *Advances in neural information processing systems*, 36:64555–64576, 2023.

Jacopo Diquigiovanni, Matteo Fontana, Simone Vantini, et al. The importance of being a band: Finite-sample exact distribution-free prediction sets for functional data. *Statistica Sinica*, 1:1–41, 2024.

John C Duchi. A few observations on sample-conditional coverage in conformal prediction. *arXiv preprint arXiv:2503.00220*, 2025.

Bengt Fornberg. Generation of finite difference formulas on arbitrarily spaced grids. *Mathematics of computation*, 51(184):699–706, 1988.

Rina Foygel Barber, Emmanuel J Candes, Aaditya Ramdas, and Ryan J Tibshirani. The limits of distribution-free conditional predictive inference. *Information and Inference: A Journal of the IMA*, 10(2):455–482, 2021.

Isaac Gibbs, John J Cherian, and Emmanuel J Candès. Conformal prediction with conditional guarantees. *Journal of the Royal Statistical Society Series B: Statistical Methodology*, page qkaf008, 2025a.

Isaac Gibbs, John J Cherian, and Emmanuel J Candès. Correcting the coverage bias of quantile regression. *arXiv preprint arXiv:2511.00820*, 2025b.

Rohan Hore and Rina Foygel Barber. Conformal prediction with local weights: randomization enables robust guarantees. *Journal of the Royal Statistical Society Series B: Statistical Methodology*, 87(2):549–578, 11 2024. ISSN 1369-7412. doi: 10.1093/rssb/qkae103.

Rafael Izbicki, Gilson Shimizu, and Rafael B Stern. Cd-split and hpd-split: Efficient conformal regions in high dimensions. *Journal of Machine Learning Research*, 23(87):1–32, 2022.

Christopher Jung, Georgy Noarov, Ramya Ramalingam, and Aaron Roth. Batch multivalid conformal prediction. In *International Conference on Learning Representations*, 2023.

Markelle Kelly, Rachel Longjohn, and Kolby Nottingham. The uci machine learning repository, 2025. URL <https://archive.ics.uci.edu>. Accessed: 2025.

Shayan Kiyani, George J. Pappas, and Hamed Hassani. Conformal prediction with learned features. In *International Conference on Machine Learning*, 2024.

Roger Koenker. *Quantile regression*, volume 38. Cambridge university press, 2005.

Jing Lei and Larry Wasserman. Distribution-free prediction bands for non-parametric regression. *Journal of the Royal Statistical Society Series B: Statistical Methodology*, 76(1):71–96, 2014.

Jing Lei, Max G’Sell, Alessandro Rinaldo, Ryan J Tibshirani, and Larry Wasserman. Distribution-free predictive inference for regression. *Journal of the American Statistical Association*, 113(523):1094–1111, 2018.

Harris Papadopoulos, Kostas Proedrou, Volodya Vovk, and Alex Gammerman. Inductive confidence machines for regression. In *European conference on machine learning*, pages 345–356. Springer, 2002.

Sangdon Park, Osbert Bastani, Nikolai Matni, and Insup Lee. Pac confidence sets for deep neural networks via calibrated prediction. In *International Conference on Learning Representations*, 2020.

Vincent Plassier, Alexander Fishkov, Victor Dheur, Mohsen Guizani, Souhaib Ben Taieb, Maxim Panov, and Eric Moulines. Rectifying conformity scores for better conditional coverage. In *International Conference on Machine Learning*, 2025a.

Vincent Plassier, Alexander Fishkov, Mohsen Guizani, Maxim Panov, and Eric Moulines. Probabilistic conformal prediction with approximate conditional validity. In *International Conference on Learning Representations*, 2025b.

Yaniv Romano, Evan Patterson, and Emmanuel Candes. Conformalized quantile regression. *Advances in neural information processing systems*, 32, 2019.

Yaniv Romano, Matteo Sesia, and Emmanuel Candes. Classification with valid and adaptive coverage. *Advances in neural information processing systems*, 33:3581–3591, 2020.

Glenn Shafer and Vladimir Vovk. A tutorial on conformal prediction. *Journal of Machine Learning Research*, 9(3), 2008.

Adith Swaminathan and Thorsten Joachims. Batch learning from logged bandit feedback through counterfactual risk minimization. *The Journal of Machine Learning Research*, 16(1):1731–1755, 2015.

Vladimir Vovk. Conditional validity of inductive conformal predictors. In *Asian conference on machine learning*, pages 475–490. PMLR, 2012.

Vladimir Vovk, Alexander Gammerman, and Glenn Shafer. *Algorithmic learning in a random world*. Springer, 2005.

Ran Xie, Rina Barber, and Emmanuel Candes. Boosted conformal prediction intervals. *Advances in Neural Information Processing Systems*, 37:71868–71899, 2024.

A Experiments Details

A.1 Dataset description

We introduce our benchmarks in alphabetical order, following the sequence presented in our tables. First, we provide a summary of all eight datasets, after which we detail each one individually. We note that the majority of these datasets are sourced from the UCI repository [Kelly et al. \[2025\]](#).

Table 3: Overview of Datasets. The feature dimension (X), label dimension (Y), and sample size (N) correspond to the pre-processed data used in the experiments.

Dataset	Feature Dim. (X)	Label Dim. (Y)	Sample Size (N)
Bike Sharing ¹	13	1	17,379
Diamonds ²	23	1	53,940
Gas Turbine ³	9	2	36,733
Naval Propulsion ⁴	16	2	11,934
SGEMM Product ⁵	14	4	50,000
Superconductivity ⁶	81	1	21,263
Transcoding ⁷	23	2	68,784
WEC (Perth) ⁸	98	49	27,000

¹ <https://archive.ics.uci.edu/dataset/275/bike+sharing+dataset>

² <https://www.kaggle.com/datasets/shivam2503/diamonds>

³ <https://archive.ics.uci.edu/dataset/551/gas+turbine+co+and+nox+emission+data+set>

⁴ <https://archive.ics.uci.edu/dataset/316/condition+based+maintenance+of+naval+propulsion+plants>

⁵ <https://archive.ics.uci.edu/dataset/440/sgemm+gpu+kernel+performance>

⁶ <https://archive.ics.uci.edu/dataset/464/superconductivity+data>

⁷ <https://archive-beta.ics.uci.edu/dataset/335/online+video+characteristics+and+transcoding+time+dataset>

⁸ <https://archive.ics.uci.edu/dataset/882/large-scale+wave+energy+farm>

Bike Sharing. This dataset pertains to urban transportation and mobility. To prevent label leakage, we removed temporal identifiers and the sub-category counts (casual and registered) from the input features. The regression target is the total count of rental bikes (cnt) recorded in the system.

Diamonds. Originating from the field of gemology and economics, this dataset is used to predict the market value of diamonds. We applied one-hot encoding to the categorical features (cut, color, clarity), dropping the first category to avoid multicollinearity. The label is the price of the diamond in US dollars.

Gas Turbine. Focusing on environmental emissions in the energy sector, this dataset aggregates sensor data from a gas turbine power plant over the period 2011–2015. The input features include various sensor measurements, while the label is a multi-dimensional vector representing Carbon Monoxide (CO) and Nitrogen Oxides (NOx) emissions.

Naval Propulsion. Used for predictive maintenance in naval engineering, this dataset contains data generated from a gas turbine propulsion plant simulator. The task involves predicting a two-dimensional label corresponding to the decay state coefficients of the GT compressor and the GT turbine.

SGEMM Product. In the domain of high-performance computing, this dataset measures the performance of matrix multiplication kernels on GPUs. Due to the massive scale of the original data, we randomly sampled $N = 50,000$ instances for our experiments. The features represent kernel parameters, and the label consists of the execution times from four independent runs.

Superconductivity. This dataset comes from material science and condensed matter physics. The input features are derived from the chemical formula and elemental properties (e.g., atomic mass, density) of various materials. The scalar regression target is the critical temperature (T_c) at which the material exhibits superconductivity.

Transcoding. Addressing cloud resource management for video processing, this dataset characterizes video transcoding tasks. We removed non-informative identifiers (such as `id` and `url`) and one-hot encoded the video codec attributes. The label is a dual-target variable comprising the transcoding time and memory usage.

WEC (Perth). Situated in the renewable energy domain, this dataset simulates the performance of a wave energy farm. The input features consist of the coordinate positions (X, Y) for 49 floating buoys. The target is a high-dimensional vector ($d_y = 49$) representing the power output generated by each individual buoy.

A.2 Baseline details

With the exception of CQR, all methods utilize the training set to learn $\hat{\mu}$ via mean squared error (MSE) minimization. The estimator $\hat{\mu}$ is parameterized by a three-layer MLP with ReLU activation. The nonconformity score is given by:

$$S(X, Y) = \|Y - \hat{\mu}(X)\|_\infty, \quad (27)$$

reducing to the standard absolute residual $S(X, Y) = |Y - \hat{\mu}(X)|$ for univariate labels.

As standard Split Conformal Prediction and Rectified Conformal Prediction (RCP) were detailed in Section 2, we proceed to introduce the other main baselines.

PLCP. Partition Learning Conformal Prediction (PLCP; [Kiyani et al., 2024](#)) aims to improve upon the marginal nature of Split CP by partitioning the feature space into **learned** regions. It optimizes these partitions to group samples of similar difficulty and applies Split CP locally within each group. This approach is formulated as a co-training procedure:

$$h^*, \mathbf{q}^* = \underset{\mathbf{q} \in \mathbb{R}^G, h \in \mathcal{H}}{\operatorname{argmin}} \frac{1}{n} \sum_{j=1}^n \sum_{i=1}^G h^i(X_j) \rho_\tau(q_i, S_j), \quad (28)$$

where G denotes the number of distinct groups (we use G to avoid conflict with the calibration sample size m , differing from the notation in [Kiyani et al., 2024](#)), and $h : \mathcal{X} \rightarrow \Delta_G$ is a partition function assigning samples to groups.

Since G is finite, provided h converges, the resulting q corresponds exactly to the empirical τ -quantile for each group. Consequently, PLCP avoids the issue discussed at the start of Section 5, namely the conformalization shift $\hat{\gamma}$ often associated with quantile regression. We report results for $G = 50$ in the main paper and provide supplementary results for $G = 20$ in Appendix [A.5](#).

Gaussian Scoring. As described in [Braun et al. \[2025a\]](#), this method assumes a multivariate Gaussian density for $Y | X$. On the training set, we train two MLPs to simultaneously predict the conditional mean $\hat{\mu}(X)$ and covariance matrix $\hat{\Sigma}(X)$ by minimizing the negative log-likelihood (NLL). The nonconformity score is defined as the Mahalanobis distance:

$$S_{\text{Mah}}(X, Y) = \left\| \hat{\Sigma}(X)^{-1/2} (Y - \hat{\mu}(X)) \right\|_2, \quad (29)$$

which reduces to the standard normalized residual $S(X, Y) = |Y - \hat{\mu}(X)|/\hat{\sigma}(X)$ [Lei et al. \[2018\]](#) when Y is one-dimensional.

CQR. Conformalized Quantile Regression (CQR; [Romano et al., 2019](#)) constructs adaptive intervals by directly estimating conditional quantiles on the training set, rather than estimating the conditional mean $\hat{\mu}$. We train two MLPs to output the lower ($\hat{q}_{\alpha/2}$) and upper ($\hat{q}_{1-\alpha/2}$) quantiles by minimizing the pinball loss. The nonconformity score is defined as:

$$S(X, Y) = \max(\hat{q}_{\alpha/2}(X) - Y, Y - \hat{q}_{1-\alpha/2}(X)). \quad (30)$$

We extend CQR to multivariate labels $Y \in \mathbb{R}^d$ by predicting the quantiles for each dimension simultaneously. In this setting, the nonconformity score is the maximum signed distance to the predicted interval boundaries across all dimensions:

$$S(X, Y) = \max_{j \in [d]} \max(\hat{q}_{\alpha/2}^{(j)}(X) - Y^{(j)}, Y^{(j)} - \hat{q}_{1-\alpha/2}^{(j)}(X)). \quad (31)$$

CQR/RCP-ALD. We begin by introducing the Asymmetric Laplace Distribution (ALD). Given a location parameter μ , scale parameter σ , and skewness parameter τ , the PDF of the ALD is:

$$f(y | \mu, \sigma, \tau) = \frac{\tau(1 - \tau)}{\sigma} \exp\left(-\frac{\rho_\tau(\mu, y)}{\sigma}\right). \quad (32)$$

Adapting this to model the conditional distribution $S | X$, we express the Maximum Likelihood Estimation (MLE) in our notation as:

$$\max_{\hat{\sigma}(x), \hat{q}(x)} \frac{1}{n} \sum_{i=1}^n \left(-\ln(\hat{\sigma}(x_i)) - \frac{\rho_\tau(\hat{q}(x_i), s_i)}{\hat{\sigma}(x_i)} \right). \quad (33)$$

As discussed in Example [3.1](#), we select the ALD as a representative of the location-scale family. Notably, the MLE for this parametric model corresponds to a weighted pinball loss, where the weights are the inverse

scale estimates $1/\hat{\sigma}(x)$. We incorporate this into CQR and RCP by replacing the standard quantile regression (pinball loss) with the ALD-based likelihood, yielding two additional baselines denoted by the suffix *-ALD*. Although we do not assume the data strictly follows an ALD, we employ this formulation as a quasi-likelihood to derive the objective function.

These two baselines are designed to isolate and examine the benefits of the approximation constructed in Proposition 3.4, effectively serving as an ablation study.

A.3 CPCP details

In this section, we provide a detailed description of the implementation, network architecture, and optimization procedure for our proposed method, **Colorful Pinball Conformal Prediction (CPCP)**.

Network architecture. To ensure the structural constraint that quantile estimates remain non-crossing (i.e., $\hat{q}_{\text{low}}(x) \leq \hat{q}_{\text{main}}(x) \leq \hat{q}_{\text{high}}(x)$), we implemented a specialized neural network architecture named `MonotonicThreeHeadNet`.

The network consists of a shared feature extractor and three specific heads:

- **Shared feature extractor:** An MLP with two hidden layers (256 units each) and ReLU activation functions.
- **Main head:** A linear layer that outputs the central quantile estimate $\hat{q}_{\text{main}}(x)$.
- **Auxiliary heads:** Two separate linear layers followed by a `Softplus` activation function to predict the positive gaps $\Delta_{\text{low}}(x)$ and $\Delta_{\text{high}}(x)$.

The final outputs are constructed as:

$$\hat{q}_{\text{low}}(x) = \hat{q}_{\text{main}}(x) - \text{Softplus}(\Delta_{\text{low}}(x)), \quad (34)$$

$$\hat{q}_{\text{high}}(x) = \hat{q}_{\text{main}}(x) + \text{Softplus}(\Delta_{\text{high}}(x)). \quad (35)$$

This parameterization strictly guarantees monotonicity and ensures that the denominator in our weight calculation remains non-negative.

Data splitting. Following Algorithm 1, we partition the calibration dataset \mathcal{D}_{cal} into three disjoint subsets:

- $\mathcal{D}_{\text{cal},1}$ (Base Training): 40% of the calibration data, used to train the three initial quantile heads.
- $\mathcal{D}_{\text{cal},2}$ (Fine-tuning): 40% of the calibration data, used to fine-tune the main head with estimated density weights.
- $\mathcal{D}_{\text{cal},3}$ (Conformalization): 20% of the calibration data, used to compute the final rectified conformity scores R_j and derive the predictive interval.

Clipping and Mixing. To prevent extreme weights from destabilizing training, we implement two regularization techniques:

- **Clipping:** The normalized weights are clamped to a maximum value (default $M = 5.0$), as detailed in Algorithm 2.
- **Loss Mixing:** The final objective function is a convex combination of the weighted loss and the original pinball loss:

$$\mathcal{L}_{\text{total}} = \lambda \mathcal{L}_{\text{weighted}} + (1 - \lambda) \mathcal{L}_{\text{pinball}}, \quad (36)$$

where λ is the mixing ratio (default $\lambda = 0.5$).

Effectively, these two strategies impose an artificial lower bound (via $\lambda = 0.5$) and upper bound ($M = 5.0$) on the normalized weights.

Quantile gap. Although we derive the non-asymptotic expression $\delta(n)$, we fix $\delta = 0.02$ throughout our experiments to avoid cherry-picking. In general, a smaller δ reduces the bias of the finite-difference estimation but requires a larger sample size to maintain stability. Our theory establishes that the optimal rate for this trade-off is $\delta^* \asymp O(n^{-1/6})$.

Algorithm 2 Colorful Pinball Conformal Prediction (Clipped Version)

- 1: **Input:** Calibration data \mathcal{D}_{cal} , Point predictor $\hat{\mu}$, Test input x_{test} , Target miscoverage level α , Bandwidth δ , Clipping multiplier M
- 2: Split \mathcal{D}_{cal} into three disjoint parts $\mathcal{D}_{\text{cal},1}$, $\mathcal{D}_{\text{cal},2}$, $\mathcal{D}_{\text{cal},3}$.
- 3: Compute conformity scores S_i for all $(x_i, y_i) \in \mathcal{D}_{\text{cal}}$.
- 4: Train three quantile estimators \hat{q}_{low} , \hat{q}_{main} , and \hat{q}_{high} (for levels $1 - \alpha - \delta$, $1 - \alpha$, $1 - \alpha + \delta$) jointly on $\mathcal{D}_{\text{cal},1}$.
- 5: Compute the raw weight for all $(x_i, y_i) \in \mathcal{D}_{\text{cal},2}$:

$$w_i \leftarrow \frac{2\delta}{\hat{q}_{\text{high}}(x_i) - \hat{q}_{\text{low}}(x_i)}.$$

- 6: Clip and normalize the weights using threshold $\tau \leftarrow M \cdot \text{mean}(\{w_j\}_{j \in \mathcal{D}_{\text{cal},2}})$:

$$w_i \leftarrow \min(w_i, \tau), \quad w_i \leftarrow w_i / \sum_{j \in \mathcal{D}_{\text{cal},2}} w_j.$$

- 7: Fine-tune the parameters of \hat{q}_{main} on $\mathcal{D}_{\text{cal},2}$ using weights w_i to get the final quantile estimator \hat{q}_τ .
- 8: Compute residuals for all $j \in \mathcal{D}_{\text{cal},3}$:

$$R_j \leftarrow S_j - \hat{q}_\tau(x_j)$$

- 9: Compute empirical quantile $\hat{\gamma}$ as the $\lceil (|\mathcal{D}_{\text{cal},3}| + 1)(1 - \alpha) \rceil$ -th smallest value of $\{R_j\}$.
- 10: **Output:** $\mathcal{C}_\alpha(x_{\text{test}}) = \{y : S(x_{\text{test}}, y) \leq \hat{\gamma} + \hat{q}_\tau(x_{\text{test}})\}$

A.4 Metric details

In summary, we consider two approaches to approximate coverage performance, based on clustering and random projection, respectively.

MSCE For MSCE, we use K-means to partition samples into K groups. There is a fundamental trade-off here: increasing K approximates the conditional coverage with finer granularity, but reduces the sample size within each group, thereby decreasing the precision of the empirical coverage estimate. Our guiding principle is to ensure sufficient samples (on the order of hundreds) within each group to evaluate coverage with percent-level precision. Consequently, we examine two settings: $K = 10$ and $K = 50$, as reported in Tables 4 and 7.

WSC For WSC, we adopt the evaluation framework of [Romano et al. \[2020\]](#), [Cauchois et al. \[2021\]](#). We first define a slab in the covariate space as:

$$S_{v,a,b} = \left\{ x \in \mathbb{R}^d \mid a \leq v^T x \leq b \right\},$$

where the direction $v \in \mathbb{R}^d$ and scalars $a < b$ are chosen to define the slice. For a predictive set \mathcal{C}_α and a threshold $\eta \in (0, 1)$, the WSC is defined as the minimum coverage over all sufficiently large slabs:

$$\text{WSC}(\mathcal{C}_\alpha; \eta) = \inf_{v \in \mathbb{R}^d, a < b} \{ \mathbb{P}[Y \in \mathcal{C}_\alpha(X) \mid X \in S_{v,a,b}] \mid \mathbb{P}[X \in S_{v,a,b}] \geq 1 - \eta \}. \quad (37)$$

In practice, we estimate WSC for a given \mathcal{C}_α by sampling 1,000 independent vectors v from the unit sphere in \mathbb{R}^d and optimizing parameters a and b via grid search. To mitigate finite-sample negative bias, we partition the test data into two disjoint subsets (e.g., with a 25%-75% split). We use the first subset to determine the optimal parameters v^*, a^*, b^* , and the second to evaluate the conditional coverage:

$$\mathbb{P}[Y \in \mathcal{C}_\alpha(X) \mid X \in S_{v^*,a^*,b^*}].$$

Volume. We report the average log-volume per dimension, calculated as $\frac{1}{d} \log \text{Volume}$. Because we utilize the infinity norm for the nonconformity score, the predictive sets for all baselines (except Gaussian scoring) are hyper-rectangles. Gaussian scoring, in contrast, produces hyper-ellipsoidal sets. Since ellipsoids are inherently more compact than hyper-rectangles, Gaussian scoring enjoys a natural advantage on this metric.

A.5 Detailed results

Table 4: Comparison of MSCE. Mean Squared Coverage Error (MSCE, \downarrow) on 8 high-dimensional benchmarks.

Method	Bike	Diamond	Gas Turbine	Naval	SGEMM	Superconductivity	Transcoding	WEC
Split	0.0030 \pm 0.0007	0.0127 \pm 0.0029	0.0033 \pm 0.0007	0.0349 \pm 0.0120	0.0035 \pm 0.0009	0.0073 \pm 0.0008	0.0045 \pm 0.0019	0.0123 \pm 0.0017
PLCP (G=20)	0.0017 \pm 0.0008	0.0022 \pm 0.0032	0.0005 \pm 0.0002	0.0248 \pm 0.0142	0.0029 \pm 0.0017	0.0015 \pm 0.0011	0.0018 \pm 0.0019	0.0024 \pm 0.0022
PLCP (G=50)	0.0018 \pm 0.0007	0.0022 \pm 0.0027	0.0008 \pm 0.0008	0.0172 \pm 0.0100	0.0028 \pm 0.0014	0.0014 \pm 0.0007	0.0034 \pm 0.0026	0.0016 \pm 0.0012
Gaussian-Scoring	0.0010 \pm 0.0005	0.0006 \pm 0.0004	0.0005 \pm 0.0002	0.0169 \pm 0.0136	0.0021 \pm 0.0028	0.0031 \pm 0.0013	0.0020 \pm 0.0019	0.0071 \pm 0.0018
CQR	0.0015 \pm 0.0010	0.0026 \pm 0.0010	0.0006 \pm 0.0004	0.0207 \pm 0.0079	0.0013 \pm 0.0005	0.0011 \pm 0.0008	0.0013 \pm 0.0013	0.0068 \pm 0.0009
CQR-ALD	0.0012 \pm 0.0010	0.0013 \pm 0.0005	0.0006 \pm 0.0003	0.0170 \pm 0.0112	0.0010 \pm 0.0005	0.0009 \pm 0.0006	0.0010 \pm 0.0005	0.0046 \pm 0.0013
RCP	0.0016 \pm 0.0005	0.0033 \pm 0.0008	0.0006 \pm 0.0003	0.0048 \pm 0.0034	0.0013 \pm 0.0003	0.0017 \pm 0.0005	0.0009 \pm 0.0005	0.0039 \pm 0.0007
RCP-ALD	0.0010 \pm 0.0004	0.0019 \pm 0.0008	0.0004 \pm 0.0002	0.0089 \pm 0.0066	0.0011 \pm 0.0004	0.0011 \pm 0.0006	0.0007 \pm 0.0003	0.0031 \pm 0.0006
CPCP	0.0011 \pm 0.0006	0.0006 \pm 0.0003	0.0005 \pm 0.0002	0.0200 \pm 0.0011	0.0003 \pm 0.0002	0.0008 \pm 0.0004	0.0010 \pm 0.0006	0.0015 \pm 0.0005
CPCP (Mix)	0.0010 \pm 0.0006	0.0005 \pm 0.0003	0.0004 \pm 0.0002	0.0021 \pm 0.0013	0.0004 \pm 0.0002	0.0008 \pm 0.0003	0.0006 \pm 0.0004	0.0011 \pm 0.0003
CPCP (Clip)	0.0009 \pm 0.0003	0.0004 \pm 0.0002	0.0004 \pm 0.0002	0.0019 \pm 0.0008	0.0003 \pm 0.0001	0.0008 \pm 0.0003	0.0005 \pm 0.0003	0.0011 \pm 0.0004
CPCP (Clip+Mix)	0.0008 \pm 0.0003	0.0004 \pm 0.0002	0.0003 \pm 0.0001	0.0017 \pm 0.0008	0.0003 \pm 0.0001	0.0007 \pm 0.0004	0.0003 \pm 0.0001	0.0010 \pm 0.0003

Table 5: Comparison of WSC. Worst-Slice Coverage (WSC, \uparrow) on 8 high-dimensional benchmarks.

Method	Bike	Diamond	Gas Turbine	Naval	SGEMM	Superconductivity	Transcoding	WEC
Split	0.8083 \pm 0.0265	0.6492 \pm 0.0180	0.8134 \pm 0.0183	0.5703 \pm 0.0574	0.7470 \pm 0.0097	0.7824 \pm 0.0237	0.7239 \pm 0.0194	0.7462 \pm 0.0165
PLCP (G=20)	0.8593 \pm 0.0286	0.8318 \pm 0.0517	0.8775 \pm 0.0176	0.6428 \pm 0.0800	0.7709 \pm 0.0494	0.8624 \pm 0.0285	0.8150 \pm 0.0472	0.8522 \pm 0.0236
PLCP (G=50)	0.8534 \pm 0.0242	0.8286 \pm 0.0585	0.8711 \pm 0.0218	0.6821 \pm 0.0925	0.7803 \pm 0.0441	0.8661 \pm 0.0218	0.7936 \pm 0.0499	0.8630 \pm 0.0198
Gaussian-Scoring	0.8605 \pm 0.0319	0.8607 \pm 0.0140	0.8727 \pm 0.0180	0.6723 \pm 0.0870	0.8251 \pm 0.0530	0.8314 \pm 0.0239	0.8287 \pm 0.0356	0.8017 \pm 0.0224
CQR	0.8653 \pm 0.0296	0.8162 \pm 0.0166	0.8752 \pm 0.0170	0.6440 \pm 0.0560	0.8284 \pm 0.0268	0.8682 \pm 0.0224	0.8313 \pm 0.0204	0.8050 \pm 0.0162
CQR-ALD	0.8699 \pm 0.0265	0.8457 \pm 0.0148	0.8750 \pm 0.0177	0.6724 \pm 0.0708	0.8462 \pm 0.0212	0.8753 \pm 0.0196	0.8378 \pm 0.0250	0.8121 \pm 0.0195
RCP	0.8662 \pm 0.0285	0.7952 \pm 0.0155	0.8780 \pm 0.0198	0.7963 \pm 0.0546	0.8291 \pm 0.0155	0.8572 \pm 0.0223	0.8272 \pm 0.0168	0.8318 \pm 0.0117
RCP-ALD	0.8722 \pm 0.0210	0.8310 \pm 0.0173	0.8860 \pm 0.0125	0.7459 \pm 0.0827	0.8360 \pm 0.0164	0.8709 \pm 0.0217	0.8570 \pm 0.0142	0.8428 \pm 0.0139
CPCP	0.8757 \pm 0.0189	0.8685 \pm 0.0173	0.8824 \pm 0.0180	0.8323 \pm 0.0374	0.8886 \pm 0.0145	0.8618 \pm 0.0205	0.8599 \pm 0.0135	0.8518 \pm 0.0192
CPCP (Mix)	0.8840 \pm 0.0235	0.8714 \pm 0.0186	0.8842 \pm 0.0161	0.8496 \pm 0.0342	0.8800 \pm 0.0125	0.8826 \pm 0.0188	0.8689 \pm 0.0139	0.8644 \pm 0.0190
CPCP (Clip)	0.8887 \pm 0.0194	0.8745 \pm 0.0100	0.8834 \pm 0.0147	0.8359 \pm 0.0338	0.8842 \pm 0.0175	0.8736 \pm 0.0142	0.8690 \pm 0.0133	0.8662 \pm 0.0197
CPCP (Clip+Mix)	0.8932 \pm 0.0142	0.8772 \pm 0.0136	0.8857 \pm 0.0126	0.8346 \pm 0.0345	0.8833 \pm 0.0138	0.8790 \pm 0.0196	0.8805 \pm 0.0124	0.8692 \pm 0.0143

B Proofs

B.1 Proof of Proposition 3.1

We fix x throughout the proof and suppress the dependence on x for notational simplicity. Let $F(\cdot) = F_{S|X=x}(\cdot)$ denote the conditional cumulative distribution function of the score $S = s(x, Y)$, and let

$$\mathcal{L}(q) = \mathbb{E}[\rho_\tau(q, S) \mid X = x]$$

denote the corresponding expected pinball loss. Let $q^* = q_\tau(x)$ be the true τ -quantile, i.e., $F(q^*) = \tau$, and let $\hat{q} = \hat{q}_\tau(x)$.

It is well known that $\mathcal{L}(\cdot)$ is a convex and absolutely continuous function of q . Moreover, for almost every $q \in \mathbb{R}$,

$$\frac{d}{dq} \mathcal{L}(q) = F(q) - \tau. \quad (38)$$

Since q^* is a minimizer of \mathcal{L} , we have $F(q^*) - \tau = 0$.

By the fundamental theorem of calculus for absolutely continuous functions, the excess risk can therefore be written as

$$\mathcal{L}(\hat{q}) - \mathcal{L}(q^*) = \int_{q^*}^{\hat{q}} (F(z) - \tau) dz. \quad (39)$$

Table 6: Comparison of Size. Average Log Volume (Size, \downarrow) on 8 high-dimensional benchmarks.

Method	Bike	Diamond	Gas Turbine	Naval	SGEMM	Superconductivity	Transcoding	WEC
Split	0.7377 \pm 0.0452	0.3924 \pm 0.0101	0.1686 \pm 0.0216	-1.1759 \pm 0.5555	-1.9751 \pm 0.0365	0.9245 \pm 0.0292	-1.5225 \pm 0.1065	1.2461 \pm 0.0246
PLCP (G=20)	0.7303 \pm 0.0618	0.3623 \pm 0.0149	0.1286 \pm 0.0185	-1.6360 \pm 0.5384	-2.0241 \pm 0.1109	0.8500 \pm 0.0285	-1.6540 \pm 0.1366	0.8960 \pm 0.1054
PLCP (G=50)	0.7129 \pm 0.0489	0.3592 \pm 0.0172	0.1287 \pm 0.0195	-1.7568 \pm 0.4563	-2.0398 \pm 0.0888	0.8417 \pm 0.0283	-1.5798 \pm 0.1398	0.8506 \pm 0.0947
Gaussian-Scoring	-0.7245 \pm 0.0568	-1.6372 \pm 0.0255	0.0378 \pm 0.0176	0.4392 \pm 0.7495	0.4323 \pm 1.2047	-0.6169 \pm 0.0347	-1.6076 \pm 0.3728	1.2466 \pm 0.2128
CQR	0.6460 \pm 0.0595	0.2813 \pm 0.0055	-0.0246 \pm 0.0162	-1.0766 \pm 0.2553	-2.5073 \pm 0.0509	0.7827 \pm 0.0181	-2.7842 \pm 0.0691	0.6652 \pm 0.0213
CQR-ALD	0.6657 \pm 0.0616	0.2920 \pm 0.0121	-0.0216 \pm 0.0187	-0.8500 \pm 0.3860	-2.6602 \pm 0.0316	0.8497 \pm 0.0325	-2.7822 \pm 0.1037	0.9686 \pm 0.0422
RCP	0.7531 \pm 0.0699	0.3222 \pm 0.0072	0.1240 \pm 0.0288	-2.1207 \pm 0.3476	-2.2085 \pm 0.0510	0.8201 \pm 0.0218	-1.8827 \pm 0.0655	0.6992 \pm 0.0367
RCP-ALD	0.7170 \pm 0.0440	0.3321 \pm 0.0083	0.1155 \pm 0.0168	-1.9556 \pm 0.4510	-2.2267 \pm 0.0491	0.8359 \pm 0.0283	-1.8650 \pm 0.0746	0.6990 \pm 0.0404
CPCP	0.7289 \pm 0.0484	0.3729 \pm 0.0151	0.1257 \pm 0.0352	-2.0808 \pm 0.3827	-2.2192 \pm 0.0543	0.8707 \pm 0.0487	-1.7002 \pm 0.1060	0.7146 \pm 0.0761
CPCP (Mix)	0.7298 \pm 0.0538	0.3760 \pm 0.0659	0.1316 \pm 0.0329	-1.9282 \pm 0.4194	-2.2567 \pm 0.0470	0.8720 \pm 0.0456	-1.7325 \pm 0.0936	0.6744 \pm 0.0550
CPCP (Clip)	0.7224 \pm 0.0379	0.3673 \pm 0.0273	0.1296 \pm 0.0306	-2.2154 \pm 0.4193	-2.2158 \pm 0.0408	0.8603 \pm 0.0346	-1.7748 \pm 0.0854	0.6569 \pm 0.0498
CPCP (Clip+Mix)	0.7384 \pm 0.0683	0.3490 \pm 0.0117	0.1258 \pm 0.0369	-2.1888 \pm 0.3348	-2.2360 \pm 0.0359	0.8455 \pm 0.0254	-1.7974 \pm 0.0713	0.6189 \pm 0.0465

Table 7: Comparison of MSCE ($K = 50$). Mean Squared Coverage Error (MSCE, \downarrow)

Method	Bike	Diamond	Gas Turbine	Naval	SGEMM	Superconductivity	Transcoding	WEC
Split	0.0071 \pm 0.0021	0.0150 \pm 0.0016	0.0054 \pm 0.0009	0.0392 \pm 0.0119	0.0065 \pm 0.0010	0.0090 \pm 0.0009	0.0108 \pm 0.0024	0.0237 \pm 0.0024
PLCP (G=20)	0.0044 \pm 0.0013	0.0043 \pm 0.0051	0.0023 \pm 0.0012	0.0290 \pm 0.0130	0.0043 \pm 0.0023	0.0045 \pm 0.0019	0.0055 \pm 0.0042	0.0057 \pm 0.0039
PLCP (G=50)	0.0041 \pm 0.0010	0.0026 \pm 0.0017	0.0021 \pm 0.0009	0.0302 \pm 0.0123	0.0037 \pm 0.0023	0.0038 \pm 0.0016	0.0073 \pm 0.0036	0.0050 \pm 0.0029
Gaussian-Scoring	0.0034 \pm 0.0011	0.0019 \pm 0.0005	0.0014 \pm 0.0003	0.0287 \pm 0.0094	0.0040 \pm 0.0044	0.0060 \pm 0.0013	0.0049 \pm 0.0076	0.6455 \pm 0.0073
CQR	0.0036 \pm 0.0014	0.0037 \pm 0.0010	0.0016 \pm 0.0006	0.0284 \pm 0.0168	0.0023 \pm 0.0007	0.0027 \pm 0.0007	0.0034 \pm 0.0016	0.0116 \pm 0.0010
CQR-ALD	0.0033 \pm 0.0010	0.0020 \pm 0.0007	0.0015 \pm 0.0005	0.0311 \pm 0.0138	0.0021 \pm 0.0013	0.0025 \pm 0.0007	0.0038 \pm 0.0020	0.0100 \pm 0.0014
RCP	0.0035 \pm 0.0011	0.0046 \pm 0.0007	0.0018 \pm 0.0003	0.0087 \pm 0.0030	0.0023 \pm 0.0003	0.0031 \pm 0.0009	0.0024 \pm 0.0006	0.0069 \pm 0.0012
RCP-ALD	0.0030 \pm 0.0006	0.0028 \pm 0.0006	0.0016 \pm 0.0005	0.0138 \pm 0.0077	0.0021 \pm 0.0005	0.0028 \pm 0.0007	0.0016 \pm 0.0003	0.0058 \pm 0.0009
CPCP	0.0032 \pm 0.0009	0.0023 \pm 0.0007	0.0016 \pm 0.0005	0.0068 \pm 0.0018	0.0010 \pm 0.0003	0.0027 \pm 0.0007	0.0029 \pm 0.0009	0.0044 \pm 0.0008
CPCP (Mix)	0.0028 \pm 0.0007	0.0018 \pm 0.0008	0.0016 \pm 0.0003	0.0073 \pm 0.0017	0.0010 \pm 0.0002	0.0028 \pm 0.0009	0.0023 \pm 0.0012	0.0038 \pm 0.0010
CPCP (Clip)	0.0029 \pm 0.0005	0.0018 \pm 0.0003	0.0015 \pm 0.0004	0.0064 \pm 0.0023	0.0011 \pm 0.0002	0.0031 \pm 0.0008	0.0020 \pm 0.0008	0.0036 \pm 0.0009
CPCP (Clip+Mix)	0.0026 \pm 0.0006	0.0014 \pm 0.0003	0.0015 \pm 0.0003	0.0059 \pm 0.0019	0.0010 \pm 0.0002	0.0025 \pm 0.0007	0.0014 \pm 0.0004	0.0034 \pm 0.0007

We now use the Lipschitz assumption on the conditional CDF. Since F is L_F -Lipschitz, it is almost everywhere differentiable with density $f(z) = F'(z)$ satisfying $f(z) \leq L_F$ for almost every z .

Without loss of generality, assume $\hat{q} \geq q^*$ (the case $\hat{q} < q^*$ follows by symmetry). Define $g(z) = F(z) - \tau$, so that $g(q^*) = 0$, $g(z) \geq 0$ for $z \geq q^*$, and $g'(z) = f(z) \leq L_F$ almost everywhere.

Consider the auxiliary function

$$H(q) = \int_{q^*}^q g(z) dz - \frac{1}{2L_F} g(q)^2, \quad q \geq q^*.$$

For almost every $q \geq q^*$, we have

$$H'(q) = g(q) \left(1 - \frac{g'(q)}{L_F} \right) = g(q) \left(1 - \frac{f(q)}{L_F} \right) \geq 0,$$

where the inequality follows from $g(q) \geq 0$ and $f(q) \leq L_F$. Since $H(q^*) = 0$ and H is non-decreasing on $[q^*, \infty)$, it follows that $H(\hat{q}) \geq 0$, i.e.,

$$\int_{q^*}^{\hat{q}} (F(z) - \tau) dz \geq \frac{1}{2L_F} (F(\hat{q}) - \tau)^2. \quad (40)$$

Combining (39) and (40) yields

$$\mathcal{L}(\hat{q}) - \mathcal{L}(q^*) \geq \frac{1}{2L_F} (F(\hat{q}) - \tau)^2,$$

which implies

$$|F(\hat{q}) - \tau| \leq \sqrt{2L_F(\mathcal{L}(\hat{q}) - \mathcal{L}(q^*))}.$$

This completes the proof. \square

B.2 Proof of Proposition 3.4

We aim to characterize the approximation error between the squared conditional coverage mismatch and the density-weighted excess risk. Let $\epsilon_q(x) := \hat{q}_\tau(x) - q_\tau(x)$ denote the estimation error.

Expansion of the Squared Coverage Error. Let $G(u) := (F_{S|X}(u) - \tau)^2$. We seek the Taylor expansion of $G(\hat{q}_\tau(x))$ around the true quantile $q_\tau(x)$. Note that $F_{S|X}(q_\tau(x)) = \tau$. We compute the derivatives of $G(u)$ evaluated at $u = q_\tau(x)$:

- First derivative:

$$G'(u) = 2(F_{S|X}(u) - \tau)f_{S|X}(u) \implies G'(q_\tau(x)) = 0. \quad (41)$$

- Second derivative:

$$G''(u) = 2f_{S|X}(u)^2 + 2(F_{S|X}(u) - \tau)f'_{S|X}(u) \implies G''(q_\tau(x)) = 2f_{S|X}(q_\tau(x))^2. \quad (42)$$

- Third derivative:

$$G'''(u) = 6f_{S|X}(u)f'_{S|X}(u) + 2(F_{S|X}(u) - \tau)f''_{S|X}(u). \quad (43)$$

Applying Taylor expansion with the Lagrange remainder to the third order:

$$\begin{aligned} (F_{S|X}(\hat{q}_\tau(x)) - \tau)^2 &= G(q_\tau(x)) + G'(q_\tau(x))\epsilon_q(x) + \frac{1}{2}G''(q_\tau(x))\epsilon_q(x)^2 + \frac{1}{6}G'''(\xi_{S,1})\epsilon_q(x)^3 \\ &= f_{S|X}(q_\tau(x))^2\epsilon_q(x)^2 + \frac{1}{6}G'''(\xi_{S,1})\epsilon_q(x)^3, \end{aligned} \quad (44)$$

where $\xi_{S,1}$ lies between $\hat{q}_\tau(x)$ and $q_\tau(x)$.

Expansion of the Excess Risk. Recall the excess risk $\mathcal{E}(x) := \mathcal{L}_x(\hat{q}_\tau(x)) - \mathcal{L}_x(q_\tau(x))$, where $\mathcal{L}_x(\cdot)$ is the expected pinball loss. The derivatives of \mathcal{L}_x at $q_\tau(x)$ are:

- $\mathcal{L}'_x(q_\tau(x)) = F_{S|X}(q_\tau(x)) - \tau = 0$.
- $\mathcal{L}''_x(q_\tau(x)) = f_{S|X}(q_\tau(x))$.
- $\mathcal{L}'''_x(u) = f'_{S|X}(u)$.

Applying Taylor's theorem to $\mathcal{E}(x)$ up to the third order:

$$\begin{aligned} \mathcal{E}(x) &= \frac{1}{2}\mathcal{L}''_x(q_\tau(x))\epsilon_q(x)^2 + \frac{1}{6}\mathcal{L}'''_x(\xi_{S,2})\epsilon_q(x)^3 \\ &= \frac{1}{2}f_{S|X}(q_\tau(x))\epsilon_q(x)^2 + \frac{1}{6}f'_{S|X}(\xi_{S,2})\epsilon_q(x)^3, \end{aligned} \quad (45)$$

where $\xi_{S,2}$ lies between $\hat{q}_\tau(x)$ and $q_\tau(x)$.

Multiplying by $2f_{S|X}(q_\tau(x))$ to match the leading term of the squared coverage error:

$$2f_{S|X}(q_\tau(x))\mathcal{E}(x) = f_{S|X}(q_\tau(x))^2\epsilon_q(x)^2 + \frac{1}{3}f_{S|X}(q_\tau(x))f'_{S|X}(\xi_{S,2})\epsilon_q(x)^3. \quad (46)$$

Characterizing the Approximation Gap. Subtracting the weighted excess risk from the squared coverage error, the second-order terms cancel out perfectly:

$$\begin{aligned} & (F_{S|X}(\hat{q}_\tau(x)) - \tau)^2 - 2f_{S|X}(q_\tau(x))\mathcal{E}(x) \\ &= \left[f_{S|X}(q_\tau(x))^2\epsilon_q(x)^2 + \frac{1}{6}G'''(\xi_{S,1})\epsilon_q(x)^3 \right] - \left[f_{S|X}(q_\tau(x))^2\epsilon_q(x)^2 + \frac{1}{3}f_{S|X}(q_\tau(x))f'_{S|X}(\xi_{S,2})\epsilon_q(x)^3 \right] \\ &= \frac{1}{6}\epsilon_q(x)^3 \left[G'''(\xi_{S,1}) - 2f_{S|X}(q_\tau(x))f'_{S|X}(\xi_{S,2}) \right]. \end{aligned} \quad (47)$$

Substituting the expression for $G'''(\xi_{S,1})$:

$$\text{Gap}(x) = \frac{1}{6}\epsilon_q(x)^3 \left[6f(\xi_{S,1})f'(\xi_{S,1}) + 2(F(\xi_{S,1}) - \tau)f''(\xi_{S,1}) - 2f(q_\tau(x))f'(\xi_{S,2}) \right], \quad (48)$$

where we abbreviated $f_{S|X}$ as f and $F_{S|X}$ as F .

We now introduce the necessary regularity assumptions as follows.

Assumption B.1 (Regularity assumption on smoothness of $f_{S|X}$). We assume that $f_{S|X}$ is second-order continuous differentiable, and there exists constants $B_w, B_f, B_{f'}, B_{f''}$ such that:

$$|f(q(x))| \leq B_w, \quad |f(\xi)| \leq B_f, \quad |f'(\xi)| \leq B_{f'}, \quad |f''(\xi)| \leq B_{f''}, \quad (49)$$

hold for each $x \in \mathcal{X}, \xi \in \mathcal{S}$, where \mathcal{S} is the space of nonconformity scores.

Here, we add a refined constant B_w because it is the bound on true weights that would appear again in Theorem 5.2.

With Assumption B.1, we have:

$$\left| (F_{S|X}(\hat{q}_\tau(x)) - \tau)^2 - 2f_{S|X}(q_\tau(x))\mathcal{E}(x) \right| \leq C_f\epsilon_q(x)^3,$$

here,

$$C_f = (6B_fB_{f'} + 2\max\{\tau, 1-\tau\}B_{f''} + 2B_wB_{f'}) .$$

This confirms that minimizing the density-weighted pinball loss is a highly accurate surrogate for minimizing the MSQE, with a negligible approximation gap in the regime of consistent quantile estimation.

□

B.3 Proof of Theorem 5.2

B.3.1 Preliminary: fast rates via local Rademacher complexity

We emphasize that Assumption 5.1 in the main text isolates only the geometric and smoothness conditions that determine the constants appearing in the excess risk bound. The fast convergence of the auxiliary quantile estimators is established separately via standard local Rademacher complexity arguments, which we briefly summarize below for completeness.

Auxiliary quantile estimation error. Recall that the quality of the estimated weights depends on the accuracy of the auxiliary quantile estimators. Define

$$\mathcal{E}_q(n) := \sup_{\beta \in \{\tau-\delta, \tau+\delta\}} \|\hat{q}_\beta - q_\beta\|_{L_2(\mathbb{P}_X)}.$$

Without additional curvature assumptions, global complexity bounds typically yield the slow rate $\mathcal{E}_q(n) = O_{\mathbb{P}}(n^{-1/4})$. To obtain fast rates, we invoke the theory of local Rademacher complexity [Bartlett et al., 2005].

Localization. For $r > 0$, define the localized hypothesis class

$$\mathcal{G}_r := \{q \in \mathcal{G} : \|q - q^*\|_{L_2(\mathbb{P}_X)} \leq r\}.$$

All subsequent arguments are restricted to \mathcal{G}_r , where r is chosen according to the fixed-point equation associated with the local Rademacher complexity.

Bernstein condition. Fast-rate results require the loss to satisfy a Bernstein (variance) condition. This property follows from the curvature of the pinball risk.

1. **Quadratic growth.** By Assumption 5.1 (density lower bound), there exists $b_w > 0$ such that $f_{S|X}(q_\tau(x) \mid x) \geq b_w$ for all $x \in \mathcal{X}$. Standard arguments for quantile regression imply that the expected pinball risk satisfies the local quadratic growth condition

$$\mathcal{R}_{\text{pin}}(q) - \mathcal{R}_{\text{pin}}(q^*) \geq \frac{b_w}{2} \|q - q^*\|_{L_2(\mathbb{P}_X)}^2, \quad \forall q \in \mathcal{G}_r.$$

2. **Variance control.** The pinball loss ρ_τ is L_ρ -Lipschitz in its prediction argument, with $L_\rho = \max(\tau, 1-\tau)$. Consequently,

$$|\rho_\tau(q, S) - \rho_\tau(q^*, S)| \leq L_\rho |q - q^*|.$$

This yields

$$\text{Var}(\rho_\tau(q, S) - \rho_\tau(q^*, S)) \leq L_\rho^2 \|q - q^*\|_{L_2(\mathbb{P}_X)}^2.$$

Combining with the quadratic growth inequality gives the Bernstein condition

$$\text{Var}(\rho_\tau(q, S) - \rho_\tau(q^*, S)) \leq B_{\text{var}} (\mathcal{R}_{\text{pin}}(q) - \mathcal{R}_{\text{pin}}(q^*)), \quad B_{\text{var}} = \frac{2L_\rho^2}{b_w}. \quad (50)$$

Fast-rate consequence. Under the Bernstein condition (50) and standard sub-root assumptions on the local Rademacher complexity (e.g., $\mathfrak{R}_n(\mathcal{G}_r) \lesssim r\sqrt{d/n}$ for VC-type classes), the fixed-point equation

$$\mathfrak{R}_n(\mathcal{G}_{r^*}) \asymp r^{*2}$$

yields $r^* \asymp \sqrt{d/n}$. As a result, the ERM-based auxiliary quantile estimators satisfy

$$\mathcal{E}_q(n) = \|\hat{q}_\beta - q_\beta\|_{L_2(\mathbb{P}_X)} \leq C_{\text{fast}} \mathfrak{R}_n(\mathcal{G}) = O_{\mathbb{P}}(n^{-1/2}),$$

uniformly over $\beta \in \{\tau - \delta, \tau + \delta\}$.

B.3.2 Error decomposition

We define the following empirical risks:

- $\mathcal{R}_n(g) := \frac{1}{n} \sum_{i=1}^n w(x_i) \rho_\tau(g(x_i), s_i)$ denotes the empirical risk with *true* weights w .
- $\hat{\mathcal{R}}_n(g) := \frac{1}{n} \sum_{i=1}^n \hat{w}(x_i) \rho_\tau(g(x_i), s_i)$ denotes the empirical risk with *estimated* weights \hat{w} .

With the classic technique in empirical process, we control the excess risk as:

$$\mathcal{R}(\hat{g}) - \mathcal{R}(g^*) \leq 2 \sup_{g \in \mathcal{G}} |\hat{\mathcal{R}}_n(g) - \mathcal{R}(g)| \tag{51}$$

$$\leq \underbrace{2 \sup_{g \in \mathcal{G}} |\mathcal{R}_n(g) - \mathcal{R}(g)|}_{\text{Term I}} + \underbrace{2 \sup_{g \in \mathcal{G}} |\hat{\mathcal{R}}_n(g) - \mathcal{R}_n(g)|}_{\text{Term II}}. \tag{52}$$

B.3.3 Bounding the stochastic error (Term I)

Term I corresponds to the generalization error with fixed (oracle) weights. To avoid imposing a uniform boundedness assumption on the loss, we introduce the following conditional sub-Gaussian assumption.

Assumption B.2 (Conditional sub-Gaussian noise). The nonconformity score S is conditionally sub-Gaussian given X . Specifically, there exists a constant $\sigma_S > 0$ such that for all $\lambda \in \mathbb{R}$,

$$\mathbb{E}[\exp(\lambda(S - \mathbb{E}[S | X])) | X] \leq \exp\left(\frac{\sigma_S^2 \lambda^2}{2}\right) \quad \text{a.s.} \tag{53}$$

By Assumption 5.1.3, the weight function satisfies $w(x) \leq B_w$ almost surely. Moreover, the pinball loss ρ_τ is L_ρ -Lipschitz in its prediction argument, where $L_\rho = \max(\tau, 1 - \tau)$. Therefore, the weighted loss

$$(x, s) \mapsto w(x) \rho_\tau(g(x), s)$$

is $B_w L_\rho$ -Lipschitz with respect to s .

Under the conditional sub-Gaussian assumption in Assumption B.2, the random variable $w(X) \rho_\tau(g(X), S)$ is conditionally sub-exponential with parameter $B_w L_\rho \sigma_S$. Applying standard global Rademacher complexity bounds together with Bernstein-type concentration inequalities yields that, with probability at least $1 - \zeta$,

$$\text{Term I} \leq 2B_w L_\rho \mathfrak{R}_n(\mathcal{G}) + B_w L_\rho \sigma_S \sqrt{\frac{2 \log(1/\zeta)}{n}}. \tag{54}$$

B.3.4 Bounding the weight estimation error (Term II)

This term captures the error arising from using estimated weights \hat{w} instead of true weights w . We bound this difference uniformly over the hypothesis class \mathcal{G} by applying the Cauchy-Schwarz inequality. The derivation proceeds as follows:

$$\begin{aligned}
\text{Term II} &:= \sup_{g \in \mathcal{G}} |\hat{\mathcal{R}}_n(g) - \mathcal{R}_n(g)| \\
&= \sup_{g \in \mathcal{G}} \left| \frac{1}{n} \sum_{i=1}^n \hat{w}(x_i) \rho_\tau(g(x_i), s_i) - \frac{1}{n} \sum_{i=1}^n w(x_i) \rho_\tau(g(x_i), s_i) \right| \\
&= \sup_{g \in \mathcal{G}} \left| \frac{1}{n} \sum_{i=1}^n (\hat{w}(x_i) - w(x_i)) \rho_\tau(g(x_i), s_i) \right| \\
&\leq \sup_{g \in \mathcal{G}} \left(\sqrt{\frac{1}{n} \sum_{i=1}^n (\hat{w}(x_i) - w(x_i))^2} \cdot \sqrt{\frac{1}{n} \sum_{i=1}^n \rho_\tau(g(x_i), s_i)^2} \right) \\
&= \left(\frac{1}{n} \sum_{i=1}^n (\hat{w}(x_i) - w(x_i))^2 \right)^{1/2} \cdot \sup_{g \in \mathcal{G}} \left(\frac{1}{n} \sum_{i=1}^n \rho_\tau(g(x_i), s_i)^2 \right)^{1/2} \\
&= \|\hat{w} - w\|_{2,n} \cdot M_{\rho, \mathcal{G}},
\end{aligned} \tag{55}$$

where $M_{\rho, \mathcal{G}} := \sup_{g \in \mathcal{G}} (\mathbb{E}_n[\rho_\tau(g, S)^2])^{1/2}$ represents the maximal empirical root-mean-square (RMS) of the loss function over the hypothesis class, and $\|\cdot\|_{2,n}$ represents the empirical L_2 -norm.

For notational convenience, we define:

$$\begin{aligned}
\Delta_\delta(x) &:= \frac{q_{\tau+\delta}(x) - q_{\tau-\delta}(x)}{2\delta} \\
\hat{\Delta}_\delta(x) &:= \frac{\hat{q}_{\tau+\delta}(x) - \hat{q}_{\tau-\delta}(x)}{2\delta},
\end{aligned} \tag{56}$$

and

$$w_\delta(x) := \frac{1}{\Delta_\delta(x)} \tag{57}$$

as the population finite-difference weight approximation.

We decompose the weight RMSE $\|\hat{w} - w\|_{L_2}$ into bias (finite difference approximation) and variance (estimation error):

$$\|\hat{w} - w\|_{2,n} \leq \|w_\delta - w\|_{2,n} + \|\hat{w} - w_\delta\|_{2,n}. \tag{58}$$

Bias analysis. We aim to bound the bias $\|w_\delta - w\|_{2,n}$ introduced by the central finite-difference approximation in a pointwise way. Recall that the target weight is the reciprocal of the quantile density function (sparsity): $w(x) = 1/q'_\tau(x)$.

First, we analyze the error of the central difference estimator $\hat{D}(x)$. Fix x and perform a Taylor expansion

with Lagrange remainder of the quantile function $q_\beta(x)$ with respect to β around τ :

$$q_{\tau+\delta}(x) = q_\tau(x) + \delta q'_\tau(x) + \frac{\delta^2}{2} q''_\tau(x) + \frac{\delta^3}{6} q'''_{\xi_1}(x), \quad (59)$$

$$q_{\tau-\delta}(x) = q_\tau(x) - \delta q'_\tau(x) + \frac{\delta^2}{2} q''_\tau(x) - \frac{\delta^3}{6} q'''_{\xi_2}(x), \quad (60)$$

where $\xi_1 \in (\tau, \tau + \delta)$ and $\xi_2 \in (\tau - \delta, \tau)$. We clarify that we fix x and use $q'_\tau(x)$ to denote the derivative of $q_\tau(x)$ w.r.t. τ .

Subtracting the two equations cancels the quadratic terms (second derivatives), yielding:

$$q_{\tau+\delta}(x) - q_{\tau-\delta}(x) = 2\delta q'_\tau(x) + \frac{\delta^3}{6} (q'''_{\xi_1}(x) + q'''_{\xi_2}(x)). \quad (61)$$

Dividing by 2δ , the error in the derivative estimation is bounded by the third derivative:

$$|\Delta_\delta(x) - q'_\tau(x)| = \left| \frac{\delta^2}{12} (q'''_{\xi_1}(x) + q'''_{\xi_2}(x)) \right| \leq \frac{\delta^2}{6} \sup_\beta |q'''_\beta(x)| \leq \frac{B_q'''}{6} \delta^2. \quad (62)$$

Here, we used Assumption 5.1.1 which bounds the third derivative of the quantile function by B_q''' .

Next, we leverage Assumption 5.1.3 ($1/q'_\tau(x) \leq B_w$) and to make the discussion meaningful, we must assume δ is small enough ($\delta \leq \sqrt{12/B_w B_q'''}$), so that:

$$\Delta_\delta(x) \geq q'_\tau(x) - |\Delta_\delta(x) - q'_\tau(x)| \geq \frac{1}{B_w} - \frac{B_q'''}{6} \delta^2 \geq \frac{1}{2B_w} \quad (63)$$

Therefore, we have

$$\begin{aligned} |w_\delta(x) - w(x)| &= \frac{|q'_\tau(x) - \Delta_\delta(x)|}{\Delta_\delta(x) q'_\tau(x)} \\ &\leq \frac{B_w^2 B_q''' \delta^2}{3}, \end{aligned} \quad (64)$$

and naturally,

$$\|w_\delta - w\|_{2,n} \leq \frac{B_w^2 B_q''' \delta^2}{3}. \quad (65)$$

Variance analysis. We aim to bound the variance term, $\|\hat{w} - w_\delta\|_{2,n}$. The problem that can not be steered around when using estimated reciprocal weights is the uniform lower bound for $\hat{\Delta}_\delta(x)$, where the uniform range is both for $x \in \mathcal{X}$ and function $\hat{q} \in \mathcal{G}$. Here, we try to weaken the needed conditions and utilize the assumption on relation between infinity norm and L_2 -norm, locally.

Assumption B.3 (Norm equivalence via Hölder regularity). Let $\mathcal{X} \subset \mathbb{R}^d$ be a compact domain with nonempty interior, and let P_X be a distribution supported on \mathcal{X} with density bounded away from zero and infinity. Assume that there exists a smoothness index $s > 0$ and a constant $R > 0$ such that for all $g \in \mathcal{G}_r$, the difference $g - g^*$ belongs to the Hölder class $C^s(\mathcal{X})$ with

$$\|g - g^*\|_{C^s(\mathcal{X})} \leq R.$$

Then there exists a constant $C_H > 0$, depending only on (s, d, \mathcal{X}, P_X) , such that for all $g \in \mathcal{G}_r$,

$$\|g - g^*\|_{L_\infty(\mathcal{X})} \leq C_H R^{\frac{d}{2s+d}} \|g - g^*\|_{L_2(P_X)}^{\frac{2s}{2s+d}}. \quad (66)$$

We note that we should consider two g^* 's, i.e., q_β for $\beta \in \{\tau \pm \delta\}$. Moreover, for notational convenience, we will denote $C_{\text{norm}} = C_H R^{\frac{d}{2s+d}}$, and $\nu = 2s/(2s+d)$.

Remark B.4. For classic statistical regression models, e.g., parametric model or Reproducing Kernel Hilbert Space (RKHS) regression with smooth kernel (e.g., Gaussian kernel), we have $\nu \approx 1$. Even for the complex ReLU multi-layer perceptrons with bounded weights and depth, functions in \mathcal{G} are piecewise linear and hence belong to the Hölder class $C^1(\mathcal{X})$ with norm bounded by a constant depending on the network architecture. In this case, Assumption B.3 applies with $s = 1$, yielding the exponent $2/(2+d)$ in (66). For other smoother activation functions such as \tanh , s would be higher.

With Assumption B.3 at hand, we can construct the uniform lower bound on $\hat{w}(x)$ with probability $1 - 2\zeta$:

$$\begin{aligned}\hat{\Delta}_\delta(x) &\geq \Delta_\delta(x) - |\Delta_\delta(x) - \hat{\Delta}(x)| \\ &\geq \Delta_\delta(x) - (|\hat{q}_{\tau+\delta}(x) - q_{\tau+\delta}(x)| + |\hat{q}_{\tau-\delta}(x) - q_{\tau-\delta}(x)|) \\ &\geq \frac{1}{2B_w} - (\|\hat{q}_{\tau+\delta} - q_{\tau+\delta}\|_{L_\infty} + \|\hat{q}_{\tau-\delta} - q_{\tau-\delta}\|_{L_\infty}) \\ &\geq \frac{1}{4B_w},\end{aligned}\tag{67}$$

For the last step, we actually need:

$$C_{\text{norm}} (C_{\text{fast}} \mathfrak{R}_n(\mathcal{G}))^\nu \leq \frac{1}{2B_w},\tag{68}$$

which translates to the a substantial lower bound on sample size n .

Thus, we have:

$$\|\hat{w} - w_\delta\|_{2,n} = \left\| \frac{\Delta_\delta - \hat{\Delta}_\delta}{\hat{\Delta}_\delta \Delta_\delta} \right\|_{2,n} \leq 8B_w^2 \|\hat{\Delta}_\delta - \Delta_\delta\|_{2,n}\tag{69}$$

To avoid reduction on rate, instead of directly bound the gap through Assumption B.3, we choose to transform the empirical norm to population norm by concentration inequality. Specifically, we define the random variable:

$$Z(X) = \left(2\delta(\hat{\Delta}_\delta(X) - \Delta_\delta(X)) \right)^2.\tag{70}$$

Since we consider $\hat{q}_\beta \in \mathcal{G}$, we can apply Assumption B.3 and control the variance of Z as:

$$\text{Var}(Z) \leq \mathbb{E}[Z^2] \leq \|Z\|_{L_\infty(\mathcal{X})} \mathbb{E}[Z] \leq C_{\text{norm}}^2 \left\| \hat{\Delta}_\delta - \Delta_\delta \right\|_{L_2}^{2+2\nu}.\tag{71}$$

Moreover, Z is also bounded, because:

$$|Z(x)| \leq \|Z\|_{L_\infty(\mathcal{X})}^2 \leq C_{\text{norm}}^2 \left\| \hat{\Delta}_\delta - \Delta_\delta \right\|_{L_2}^{2\nu} \leq C_{\text{norm}}^2 \mathcal{E}_q(n)^{2\nu}\tag{72}$$

Hence, we can applying Bernstein's inequality [Bach, 2024] to transform the empirical norm into population

norm, with probability at least $1 - \zeta$:

$$\begin{aligned}
\|2\delta(\hat{\Delta}_\delta - \Delta_\delta)\|_{2,n}^2 &\leq \|2\delta(\hat{\Delta}_\delta - \Delta_\delta)\|_{L_2}^2 + \sqrt{\frac{2\left(C_{\text{norm}}^2 \|\hat{\Delta}_\delta - \Delta_\delta\|_{L_2}^{2+2\nu}\right) \log(1/\zeta)}{n}} + \frac{2C_{\text{norm}}^2 \mathcal{E}_q(n)^{2\nu} \log(1/\zeta)}{3n} \\
&\leq 2\mathcal{E}_q(n)^2 + C_{\text{norm}} \mathcal{E}_q(n)^{1+\nu} \sqrt{\frac{2^{3+2\nu} \log(1/\zeta)}{n}} + \frac{2C_{\text{norm}}^2 \mathcal{E}_q(n)^{2\nu} \log(1/\zeta)}{3n}.
\end{aligned} \tag{73}$$

B.3.5 Optimal bandwidth and final bound

Combining the bias and variance terms derived above, the error Term II can be written as $U(\delta)$:

$$U(\delta) = M_{\rho, \mathcal{G}}(c_1 \delta^2 + c_2 \delta^{-1}),$$

where

$$c_1 = \frac{B_w^2 B_q'''}{3}, \tag{74}$$

and

$$c_2 = 4B_w^2 \sqrt{2\mathcal{E}_q(n)^2 + C_{\text{norm}} \mathcal{E}_q(n)^{1+\nu} \sqrt{\frac{2^{3+2\nu} \log(1/\zeta)}{n}} + \frac{2C_{\text{norm}}^2 \mathcal{E}_q(n)^{2\nu} \log(1/\zeta)}{3n}}. \tag{75}$$

Minimizing $U(\delta)$ with respect to δ yields the optimal bandwidth

$$\delta^* = \left(\frac{c_2}{2c_1}\right)^{1/3}.$$

Substituting δ^* back into $U(\delta)$, we obtain

$$\begin{aligned}
U(\delta^*)/M_{\rho, \mathcal{G}} &= 3\left(\frac{c_1}{2}\right)^{1/3} c_2^{2/3} \\
&= C_{\text{const}} B_w^2 (B_q''')^{1/3} \left(2\mathcal{E}_q(n)^2 + C_{\text{norm}} \mathcal{E}_q(n)^{1+\nu} \sqrt{\frac{2^{3+2\nu} \log(1/\zeta)}{n}} + \frac{2C_{\text{norm}}^2 \mathcal{E}_q(n)^{2\nu} \log(1/\zeta)}{3n}\right)^{1/3},
\end{aligned} \tag{76}$$

where $C_{\text{const}} = 2 \times 3^{2/3}$.

We now invoke the fast-rate guarantee in the local neighborhood \mathcal{G}_r . Specifically, under the local Rademacher complexity condition,

$$\mathcal{E}_q(n) = \|\hat{q}_\beta - q_\beta\|_{L_2(P_X)} \leq C_{\text{fast}} \mathfrak{R}_n(\mathcal{G}) = O(n^{-1/2}) \tag{77}$$

with probability at least $1 - \zeta$.

We conclude that

$$U(\delta^*)/M_{\rho, \mathcal{G}} = O\left(\mathfrak{R}_n(\mathcal{G})^{2/3}\right),$$

and in particular,

$$U(\delta^*) = O(n^{-1/3}),$$

with probability at least $1 - 2\zeta$.

Hence, incorporating Term I and Term II, with probability at least $1 - 3\zeta$, we have the final bound on the generalization error $\mathcal{R}(\hat{g}) - \mathcal{R}(g^*)$:

$$\begin{aligned} \mathcal{R}(\hat{g}) - \mathcal{R}(g^*) &\leq 2(\text{Term I} + \text{Term II}) \\ &\leq 4B_w L_\rho \mathfrak{R}_n(\mathcal{G}) + 2B_w L_\rho \sigma_S \sqrt{\frac{2 \log(1/\zeta)}{n}} \\ &\quad + 2M_{\rho, \mathcal{G}} C_{\text{const}} B_w^2 (B_q''')^{1/3} \left(2\mathcal{E}_q(n)^2 + C_{\text{norm}} \mathcal{E}_q(n)^{1+\nu} \sqrt{\frac{2^{3+2\nu} \log(1/\zeta)}{n}} + \frac{2C_{\text{norm}}^2 \mathcal{E}_q(n)^{2\nu} \log(1/\zeta)}{3n} \right)^{1/3} \end{aligned} \quad (78)$$

It is easy to check that the weight estimation error is the leading term with appropriately large n . Hence, we conclude that:

$$\mathcal{R}(\hat{g}) - \mathcal{R}(g^*) = O(\mathfrak{R}_n(\mathcal{G})^{2/3}), \quad (79)$$

which implies

$$\mathcal{R}(\hat{g}) - \mathcal{R}(g^*) = O(n^{-1/3}). \quad (80)$$

Remark B.5. The probability $1 - 3\zeta$ follows from a union bound over three high-probability events: one controlling the generalization error in Term I, and two ensuring that the auxiliary estimators $\hat{q}_{\tau+\delta}$ and $\hat{q}_{\tau-\delta}$ remain within the prescribed L_2 -neighborhoods of $q_{\tau+\delta}$ and $q_{\tau-\delta}$, respectively.

□

B.4 Proof of Hölder-type Norm Equivalence

Lemma B.6 (Norm equivalence for Hölder classes). *Let $\mathcal{X} \subset \mathbb{R}^d$ be compact with nonempty interior, and let P_X be a distribution supported on \mathcal{X} whose density is bounded away from zero and infinity. Suppose $h \in C^s(\mathcal{X})$ for some $s \in (0, 1]$ and*

$$\|h\|_{C^s(\mathcal{X})} \leq R.$$

Then there exists a constant $C_H > 0$, depending only on (s, d, \mathcal{X}, P_X) , such that

$$\|h\|_{L_\infty(\mathcal{X})} \leq C_H R^{\frac{d}{2s+d}} \|h\|_{L_2(P_X)}^{\frac{2s}{2s+d}}. \quad (81)$$

Proof. Fix any $x_0 \in \mathcal{X}$. By the Hölder continuity of h and the reverse triangle inequality, for all $x \in \mathcal{X}$, we have $|h(x)| \geq |h(x_0)| - R\|x - x_0\|^s$. Let $B(x_0, r)$ denote the Euclidean ball of radius $r > 0$ centered at x_0 . Assuming r is small enough such that $|h(x_0)| > Rr^s$, we can lower bound the L_2 -norm on this local ball:

$$\|h\|_{L_2(P_X)}^2 \geq \int_{B(x_0, r) \cap \mathcal{X}} h(x)^2 dP_X(x) \gtrsim r^d (|h(x_0)| - Rr^s)^2, \quad (82)$$

where the implicit constant depends on the density of P_X and the geometry of \mathcal{X} . Taking the square root and rearranging terms to isolate $|h(x_0)|$ yields the bias-variance decomposition:

$$|h(x_0)| \lesssim \underbrace{Rr^s}_{\text{bias}} + \underbrace{\|h\|_{L_2(P_X)} r^{-d/2}}_{\text{variance proxy}}. \quad (83)$$

(Note: If $|h(x_0)| \leq Rr^s$, this inequality holds trivially). We optimize the right-hand side over $r > 0$ by choosing the balancing radius:

$$r \asymp \left(\frac{\|h\|_{L_2(P_X)}}{R} \right)^{\frac{2s}{2s+d}}. \quad (84)$$

Substituting (84) back into (83), we obtain

$$|h(x_0)| \lesssim R^{\frac{d}{2s+d}} \|h\|_{L_2(P_X)}^{\frac{2s}{2s+d}}.$$

Since x_0 is arbitrary, taking the supremum over $x_0 \in \mathcal{X}$ completes the proof. \square

Remark B.7 (Connection to Gagliardo-Nirenberg Inequality). The inequality (81) constitutes a specific instance of the celebrated Gagliardo-Nirenberg interpolation inequality. In its general form on a bounded domain satisfying the cone condition, for indices $1 \leq q, r \leq \infty$ and $j < m$, the inequality states:

$$\|D^j u\|_{L_p} \leq C_1 \|D^m u\|_{L_r}^\theta \|u\|_{L_q}^{1-\theta} + C_2 \|u\|_{L_q}. \quad (85)$$

In our setting, we aim to bound the function value ($j = 0$) in the L_∞ -norm ($p = \infty$) using the L_2 -norm ($q = 2$). The Hölder smoothness constraint $\|\cdot\|_{C^s} \leq R$ serves as the high-order derivative control, corresponding to the limiting case of Sobolev regularity with $m = s$ and $r = \infty$. The interpolation parameter θ is governed by the dimensional scaling relation:

$$\begin{aligned} \frac{1}{p} &= \frac{j}{d} + \theta \left(\frac{1}{r} - \frac{m}{d} \right) + \frac{1-\theta}{q} \\ \implies 0 &= 0 + \theta \left(0 - \frac{s}{d} \right) + \frac{1-\theta}{2}. \end{aligned} \quad (86)$$

Solving (86) for θ yields $\theta = \frac{d}{2s+d}$. Consequently, the exponent for the L_2 -term is $1 - \theta = \frac{2s}{2s+d}$, which precisely matches the rate in (81).

C Supplementary Material

C.1 Gap between $F_{S|X}(\hat{q}(x))$ and $\pi(x)$

In this part, we supplement the results proved in [Plassier et al. \[2025a\]](#).

Assumption C.1. Let $R = S - \hat{q}_\tau(X)$ be the random variable representing the residuals of scores. We assume the density f_R and $f_{R|X}$ exists for each $x \in \mathcal{X}$, and the likelihood ratio is bounded for each $x \in \mathcal{X}$:

$$\sup_{r \in \mathbb{R}} \frac{f_{R|X=x}(r)}{f_R(r)} \leq \Lambda.$$

Here, we adopt a slightly stronger ² version than [Plassier et al. \[2025a\]](#) and suppress complex notations to enhance the readability. Assumption C.1 essentially characterizes the quality of quantile estimator, i.e., to what extent the quantile estimator removes the covariate-dependency on scores.

Theorem C.2 (Theorem 2 in [Plassier et al. \[2025a\]](#)). *Suppose Assumption C.1 holds. For any target level τ such that $(1 - \tau) \in ((m + 1)^{-1}, 1)$, the deviation between the true and implied coverage is bounded by:*

$$-\Delta_{m,\tau}^- \leq \pi(x) - F_{S|X}(\hat{q}_\tau(x)) \leq \Delta_{m,\tau}^+, \quad (87)$$

where the strictly positive slack terms are given by:

$$\Delta_{m,\alpha}^- = \Lambda \left(1 - \frac{k_{cal}}{m + 1} \right) [F_R(0)]^{m+1}, \quad (88)$$

$$\Delta_{n,\alpha}^+ = \Lambda \left(\frac{k_{cal}}{m + 1} \right) [1 - F_R(0)]^{m+1}, \quad (89)$$

with $k_{cal} = \lceil (m + 1)(1 - \alpha) \rceil$ being the conformal score rank, and $F_R(0) = \mathbb{P}(S \leq \hat{q}_\tau(X))$ being the marginal coverage of the uncalibrated estimator.

Remark C.3. Since we assume the consistency of \hat{q}_τ , we have $F_R(0)$ converges to τ in probability. Thus, the slack terms decay exponentially with n , implying that $F_{S|X}(\hat{q}_\tau(x))$ converges exponentially fast to $\pi(x)$.

We note that the conformalization step is still substantial when n is small (e.g., smaller than 100), while the Λ would also decrease with the increase of the quality of the quantile estimator (and originally, the size of samples used for training the quantile estimator). Hence, with a reasonably large sample size of \mathcal{D}_{cal} , we can focus on characterizing the finite-sample performance of our method through analyzing the MSE of $F_{S|X}(\hat{q}_\tau(x))$, and naturally the surrogate, expected risk of density-weighted pinball loss. We now present our main assumptions and theorem as follows.

²We assume the existence of PDF, while in [Plassier et al. \[2025a\]](#), the continuity of CDF is assumed.